J. Fluid Mech. (2017), *vol.* 827, *pp.* 664–693.
doi:10.1017/jfm.2017.438

Thermoacoustic instability as mutual synchronization between the acoustic field of the confinement and turbulent reactive flow

Samadhan A. Pawar[1,†], Akshay Seshadri[1], Vishnu R. Unni[1] and R. I. Sujith[1]

[1]Indian Institute of Technology Madras, Chennai - 600 036, India

(Received 18 August 2016; revised 13 June 2017; accepted 20 June 2017;
first published online 29 August 2017)

Thermoacoustic instability is the result of a positive coupling between the acoustic field in the duct and the heat release rate fluctuations from the flame. Recently, in several turbulent combustors, it has been observed that the onset of thermoacoustic instability is preceded by intermittent oscillations, which consist of bursts of periodic oscillations amidst regions of aperiodic oscillations. Quantitative analysis of the intermittency route to thermoacoustic instability has been performed hitherto using the pressure oscillations alone. We perform experiments on a laboratory-scale bluff-body-stabilized turbulent combustor with a backward-facing step at the inlet to obtain simultaneous data of acoustic pressure and heat release rate fluctuations. With this, we show that the onset of thermoacoustic instability is a phenomenon of mutual synchronization between the acoustic pressure and the heat release rate signals, thus emphasizing the importance of the coupling between these non-identical oscillators. We demonstrate that the stable operation corresponds to desynchronized aperiodic oscillations, which, with an increase in the mean velocity of the flow, transition to synchronized periodic oscillations. In between these states, there exists a state of intermittent phase synchronized oscillations, wherein the two oscillators are synchronized during the periodic epochs and desynchronized during the aperiodic epochs of their oscillations. Furthermore, we discover two different types of limit cycle oscillations in our system. We notice a significant increase in the linear correlation between the acoustic pressure and the heat release rate oscillations during the transition from a lower-amplitude limit cycle to a higher-amplitude limit cycle. Further, we present a phenomenological model that qualitatively captures all of the dynamical states of synchronization observed in the experiment. Our analysis shows that the times at which vortices that are shed from the inlet step reach the bluff body play a dominant role in determining the behaviour of the limit cycle oscillations.

Key words: acoustics, nonlinear dynamical systems, turbulent reacting flows

1. Introduction

Characterization of the transition of combustion systems from stable to unstable operation has been a topic of intense research during recent times (Lieuwen 2002;

† Email address for correspondence: samadhanpawar@ymail.com

Gotoda *et al.* 2011; Kabiraj *et al.* 2012*a*; Nair, Thampi & Sujith 2014). The unstable operation, which corresponds to large-amplitude self-sustained periodic oscillations, goes by the name of thermoacoustic instability. Such instabilities arise as a result of a positive feedback between hydrodynamics, acoustics and combustion processes occurring in a combustor (Lieuwen & Yang 2005). The coupled interaction of these processes plays a major role in both the generation and the sustenance of these instabilities (McManus, Poinsot & Candel 1993; Sujith, Juniper & Schmid 2016). Researchers have attempted to understand the intricacies involved in such interactions, and have subsequently exploited the acquired knowledge to devise techniques that either mitigate the strength of such oscillations (Putnam 1971; Schadow & Gutmark 1992; McManus *et al.* 1993) or forewarn their onset (Lieuwen 2005; Nair *et al.* 2013; Gotoda *et al.* 2014; Nair & Sujith 2014).

Nonlinearities play a significant role in the genesis of thermoacoustic instabilities of gas turbine combustors (Culick 1976; Lieuwen 2003*a*). Due to the small amplitude of the acoustic oscillations in the combustor relative to the mean pressure, the acoustic oscillations in the duct are presumed to behave in a linear fashion (Dowling 1997). The nonlinearity, then mainly stems from the nature of the interaction between the heat release rate fluctuations and the acoustic field (Dowling 1997). The nonlinear behaviour of these coupled processes is evident in the unstable operation of combustors, which is known to be limit cycle oscillations (Culick 1994). Dynamical systems theory has fostered the understanding of such nonlinear phenomena. Using this theory, the diverse dynamical behaviour exhibited by a thermoacoustic system has been brought to light (Sterling 1993; Jahnke & Culick 1994; Datta *et al.* 2009; Gotoda *et al.* 2011; Kabiraj & Sujith 2012; Kabiraj *et al.* 2012*a*). In the parlance of dynamical systems theory, the transition of combustion systems from stable to unstable operation is the result of a bifurcation (Lieuwen 2002; Ananthkrishnan, Deo & Culick 2005; Subramanian *et al.* 2010; Gotoda *et al.* 2011; Kabiraj *et al.* 2012*a*).

Jahnke & Culick (1994), in their model of a solid rocket motor, were the first to observe the bifurcation of limit cycle oscillations to a quasiperiodic state through the birth of a torus. The period doubling route to chaos was observed by Sterling (1993), Datta *et al.* (2009) and Lei & Turan (2009) in their modelling studies, by incorporating different models for combustion. Kabiraj and co-workers performed an experimental analysis that showed different dynamical states (2012; 2012*a*) and the route to chaos (2012*b*) in a thermoacoustic system. They witnessed the presence of period-k, quasiperiodic, frequency locked, chaotic and limit cycle oscillations in a ducted laminar flame combustor. Furthermore, Subramanian (2011) and Kashinath, Waugh & Juniper (2014) reported similar results in their numerical simulation of a premixed flame system, for different choices of control parameters.

In the case of turbulent combustion systems, the passage to thermoacoustic instability has traditionally been reported as a transition of the combustor from a stable (combustion noise) to an unstable (limit cycle) state (Lieuwen 2002). Nair & Sujith (2013), however, reported the presence of a state called intermittency prior to the onset of limit cycle oscillations in their system. Intermittency here is a dynamical state consisting of an apparently irregular appearance of bursts of large-amplitude periodic oscillations among regions of aperiodic oscillations (Nair *et al.* 2014). Thenceforth, numerous studies have reported the presence of such intermittent oscillations prior to the onset of limit cycle oscillations in a variety of turbulent combustion systems (Gotoda *et al.* 2014; Murugesan & Sujith 2015*b*; Unni & Sujith 2015; Pawar *et al.* 2016; Wilhite *et al.* 2016).

Since the emergence of limit cycle oscillations is of prime concern in combustion systems, there are studies dedicated to understanding the nature of the transition to

periodic oscillations. Lieuwen (2002) viewed such a transition of a thermoacoustic system as the loss of stability of a stable fixed point, along with the generation of a noisy elliptic structure in the phase space. Nair & Sujith (2014) viewed the transition of combustion noise to limit cycle oscillations as the loss of the multifractal signature of the system upon the emergence of order. Murugesan & Sujith (2015*a*), on the other hand, analysed the transition behaviour of combustion dynamics using complex network theory. They discovered that the scale-free nature of the network observed during combustion noise vanishes upon the onset of thermoacoustic instability.

Despite achieving some success in characterizing the transition, all of these studies relied on analysing the acoustic pressure oscillations alone. However, it is well known that the generation of thermoacoustic instability is a coupled response of the acoustic oscillations and the heat release fluctuations present in the combustor (Rayleigh 1878). The inherent fluctuations present in the turbulent flow field perturb the flame. The resultant fluctuations in the heat release rate affect the acoustic waves, which, after reflection from the boundaries, alter the heat release rate further, establishing a feedback loop (Lieuwen & Yang 2005).

In some systems, the presence of vortex shedding enhances this feedback (Smith & Zukoski 1985; Poinsot *et al.* 1987). Such coupled interaction between the duct acoustics and the flame dynamics or the heat release rate fluctuations in a turbulent combustor has been analysed by various researchers (Rogers 1956; Keller *et al.* 1982; Smith & Zukoski 1985; Poinsot *et al.* 1987; Sterling & Zukoski 1987; Yu, Trouve & Daily 1991; Macquisten & Dowling 1993; Broda *et al.* 1998; Venkataraman *et al.* 1999; Guethe & Schuermans 2007; Sivakumar & Chakravarthy 2008). It is evident from these studies that the coupling between these phenomena is at the core of what gives rise to the observed dynamics. The focus of these studies, however, was limited to just stable and unstable operation of the combustor. None of the studies quantitatively analysed the relationship between the acoustic field and heat release rate fluctuations during the transition from combustion noise to limit cycle oscillations. The observation of locking of the acoustic and heat release rate fluctuations at the onset of limit cycle oscillations naturally motivates one to examine the presence of synchronization in the system. In order to investigate the coupled behaviour of these components of a thermoacoustic system, we adopt the framework of synchronization theory.

Synchronization, in simple terms, is the matching of the rhythm of oscillators upon coupling. In the seventeenth century, Huygens discovered this universal phenomenon while observing the locking of beats of two pendulum clocks hung over a wall (Pikovsky, Rosenblum & Kurths 2003). In the ensuing years, this phenomenon has been observed in a variety of disciplines ranging from biology (Leon 2001), ecosystems (Blasius, Amit & Lewi 1999), chemistry (Schreiber & Marek 1982), communication (Kocarev & Parlitz 1995) to various types of engineering systems (Heagy, Carroll & Pecora 1994; Roy & Thornburg 1994). The strength of the mutual interaction between the coupled oscillators is a crucial parameter that determines their arrival at a common frequency or at a constant phase difference.

Synchronization among oscillators is usually examined by investigating the locking of phase (or frequency) of their signals (Pikovsky *et al.* 2003). The phenomenon of synchronization is common to periodic (Blekhman, Landa & Rosenblum 1995) as well as chaotic oscillators (Boccaletti *et al.* 2002). The synchronization of periodic oscillators may be expected, but the fact that chaotic oscillators can synchronize, even for different initial conditions, is fascinating and surprising, given their sensitive dependence on the initial conditions. A system of coupled chaotic oscillators that are

initially desynchronized can become synchronized by means of varying the coupling strength (Boccaletti *et al.* 2002), through periodic forcing, or feedback (Wen, Kiss & Hudson 2001). However, in real physical systems, different types of coupling mechanisms can exist simultaneously, due to which it is difficult to identify the effect of each individual coupling mechanism on the dynamics of the system.

In the case of complex fluid systems, there are instances where the features of synchronization have been observed (Zdravkovich 1982; Gunnoo, Abcha & Ezersky 2016). The synchronized shedding of large-scale coherent structures with the vibrating bodies is a well-known phenomenon in studies involving flow-induced vibrations (Green 1995). When the fluid flows over a bluff body, a vortex street is generated in its wake region, commonly known as the von Kármán vortex street. The shedding of a vortex induces vibration in the bluff body, which, in turn, affects the shedding process. When the frequency of vortex shedding is close to or equal to the frequency of natural oscillations of the bluff body, the frequency of vortex shedding locks in with that of the bluff body. Such lock-in results in the synchronized generation of vortex streets in the wake region of the bluff body. The lock-in mechanism alters the vortex shedding pattern (Zdravkovich 1982), increases the spanwise correlation in the wake and shifts the vortex shedding frequency to the frequency of the vibrating body (Griffin & Ramberg 1974; Blevins 1985; Williamson & Roshko 1988; Griffin & Hall 1991). Thus, in the region of lock-in, the interaction between the flow and the vibrating body controls the shedding pattern of the large-scale structures. Although these studies do not compute the phase to check for synchronization, it seems very likely that they exhibit phase locking.

Similarly, in the case of a thermoacoustic system with an underlying turbulent flow field, there seems to be a presence of synchronized behaviour between two coupled processes, namely the acoustic field in the duct and the turbulent reactive flow fluctuations present in the system, at the onset of thermoacoustic instability. In this state, a vortex is shed in the combustor after every acoustic cycle (Crump *et al.* 1986; Poinsot *et al.* 1987; Yu *et al.* 1991). Chakravarthy, Sivakumar & Shreenivasan (2007) referred to such interaction between the vortex shedding (hydrodynamic) and the acoustic field during the onset of limit cycle oscillations as a phenomenon of vortex–acoustic lock-on. During this process, they reported the shifting of the frequency of acoustic oscillations in the duct to the frequency of vortex shedding in the system. Bellows, Hreiz & Lieuwen (2008), on the other hand, investigated the lock-in mechanism of a thermoacoustic system by studying its response to an external periodic forcing. In this case, when the frequency of external forcing is sufficiently close to the natural frequency of the system, or when the amplitude of forcing is high enough, the system dynamics locks in to the external forcing (Bellows *et al.* 2008; Thumuluru & Lieuwen 2009; Balusamy *et al.* 2015). These studies, however, do not focus on the intermittency route observed in a turbulent combustion system, and neither do they utilize many of the tools used in synchronization theory. We aim to fill these gaps.

In the present study, we view thermoacoustic instability as a synchronization phenomenon between two mutually coupled non-identical oscillators, namely the acoustic field and the turbulent reactive flow present in the combustor. We show that the two-way coupling between these oscillators results in adjustment of their rhythm to a common frequency at a particular value of the control parameter. Using the framework of synchronization theory, we establish a new description for the intermittency route through which a combustor with a turbulent reacting flow field transitions from a stable to an unstable state of operation. We believe that the

approach of viewing thermoacoustic instability, in such systems with turbulent reactive flow, as synchronization of two mutually coupled oscillators gives more insight into understanding the complex interactions between the coupled processes of the system. With the help of this approach, we show that the onset of thermoacoustic instability is not just a locking of the dominant frequencies of both of the oscillators, but also the locking of their instantaneous phases. We present a phenomenological model that qualitatively describes the dynamics of the combustion system used in the present study. Furthermore, the theoretical analysis sheds light on the role of vortex shedding in the generation of different states of synchronization in the thermoacoustic system.

The rest of the paper is arranged as follows. In § 2, we briefly describe the analysis of synchronization of two coupled oscillators. The details of the experimental set-up and the procedures for analysing the experimental data are provided in § 3. The results and discussion are presented in § 4. In § 5, the description of the model and the corresponding results and discussion are presented. Finally, the conclusions of the present study are summarized in § 6.

2. Synchronization of coupled oscillators

Synchronization of coupled chaotic oscillators has been mainly categorized into phase synchronization (Rosenblum, Pikovsky & Kurths 1996), lag synchronization (Rosenblum, Pikovsky & Kurths 1997), complete synchronization (Fujisaka & Yamada 1983) and generalized synchronization (Rulkov *et al.* 1995). In phase synchronization, both of the oscillators of a coupled system show perfect locking in their phases; however, their amplitudes remain uncorrelated. During lag and complete synchronization, both the amplitudes and the phases of the signals from the coupled oscillators display exactly the same behaviour. The only difference is that, in lag synchronization, the phases of the signals are lagged by a constant value of time, whereas, in complete synchronization, the signals are in phase with each other. In the case of generalized synchronization, there exists a functional relationship between the signals of coupled oscillators. In some cases, the state of perfect synchronization is preceded by a state of intermittent synchronization, wherein regions of synchronized and desynchronized oscillations are simultaneously present in the signal (Sungwoo, Park & Rubchinsky 2011).

2.1. *Calculation of instantaneous properties of the signal*

The phase of a signal is an important parameter in analysing the synchronization characteristics of coupled oscillator systems. Various methods are available in the literature to calculate the instantaneous phase of a signal (Pikovsky *et al.* 2003); however, the choice of a specific method depends on the properties of the signal. One of the ways to calculate the instantaneous quantity (amplitude or phase) of a signal is to use an analytic signal approach (Gabor 1946) based on the Hilbert transform (Rosenblum *et al.* 1996). The analytic signal ($\zeta(t)$) is a complex quantity, whose real part is the original signal ($s(t)$) and whose imaginary part is the Hilbert transform ($s_H(t) = (1/\pi)\ \text{P.V.}\ \int_{-\infty}^{\infty} (s(\tau)/(t-\tau))\,\mathrm{d}\tau$) of it, where P.V. is the Cauchy principal value of the integral. Thus, the analytic signal is defined as

$$\zeta(t) = s(t) + \mathrm{i}s_H(t) = A(t)\mathrm{e}^{\mathrm{i}\phi(t)}, \tag{2.1}$$

where $\phi(t)$ represents the instantaneous phase and $A(t)$ the instantaneous amplitude of the signal.

The synchronization feature of coupled oscillators is investigated by analysing the temporal variation of their relative phase and is calculated as $\Delta\phi_{i,j}(t) = \phi_j(t) - \phi_i(t)$. The condition for phase locking is $|\Delta\phi_{i,j}(t)| = \text{const.}$ (where const. $< 2\pi$), which means that the phase difference between the signals remains bounded during the state of synchronization. In an ideal case, synchronization leads to a constant value of the relative phase, which can be zero (for complete synchronization) or some non-zero value (for other types of synchronization). However, in practice, most of the signals are contaminated with noise; their relative phases show fluctuations around some constant value of phase shift.

Although the analytic signal approach is desirable, as it gives us the phase at every time instant, there are limitations in calculating the instantaneous phase by this technique. First, it works well only for narrow-band signals and, second, the calculated phase has physical meaning only if the projection of a signal in the analytic plane (plot between the real and imaginary parts of the analytic signal) has a unique centre of rotation (Yalçinkaya & Lai 1997). If the attractor of a signal possesses a unique centre of rotation in the analytic plane, it is termed a phase-coherent attractor; otherwise, it is referred to as a non-phase-coherent attractor (Yalçinkaya & Lai 1997; Lakshmanan & Senthilkumar 2011). In our system, for the signals acquired during the combustion noise and intermittency state, we notice the presence of non-phase-coherent attractors (the figures are not shown here). The presence of multiple centres of rotation makes it difficult to select a single reference point and thereby define an instantaneous phase around it. Conversely, in the case of limit cycle oscillations, we observe a single centre of rotation (phase-coherent attractor) in the analytic plane, and, thus, the instantaneous Hilbert phase is well defined.

Among the very few methods available in the literature that characterize the synchronization features of non-phase-coherent signals (Yalçinkaya & Lai 1997; Osipov *et al.* 2003; Romano *et al.* 2005), we use a method based on recurrence plots (Romano *et al.* 2005) in the present study. The advantage of this method over others is that it does not require a plane over which the state space trajectory has to rotate about the unique point. In addition, this method can be used for signals that are non-stationary and ones that are contaminated with noise. The reconstruction of the phase space ensures that the attractor is untangled, as the trajectories in the phase space do not intersect with each other. Since this method is based on the recurrence property of such a trajectory, it eliminates the need to seek a centre of rotation (Romano *et al.* 2005).

2.2. *Analysis of synchronization using recurrence theory*

Recurrence is a fundamental property of a deterministic dynamical system (Eckmann, Kamphorst & Ruelle 1987). The recurrence in the dynamics of the system can be effectively represented by using a two-dimensional binary matrix, known as a recurrence plot (RP) (Marwan *et al.* 2007). The construction of an RP relies on reconstruction of the phase space, which is possible on account of Takens' delay embedding theorem (Takens 1981). The time series of an experimental observable, for example unsteady pressure oscillations $\{p'(t) = p'_1, p'_2, p'_3, \ldots, p'_N\}$, measured at a particular value of the control parameter is embedded in the phase space by choosing a suitable value of the time delay (T) and a minimum embedding dimension (E) (Abarbanel 1996). The embedding dimension is obtained from the method suggested by Cao (1997), whereas the optimum value of the time delay is chosen as the first minimum of the average mutual information (Fraser & Swinney 1986). The details

of the phase space reconstruction applied to thermoacoustic systems are available in Kabiraj *et al.* (2012*a*) and Nair & Sujith (2013).

An important parameter required in the construction of an RP is the cutoff threshold (ε), which is instrumental in deciding the recurrence of the phase space trajectory (Schinkel, Dimigen & Marwan 2008). We can choose the threshold as a fraction of the size of the attractor, or assign it values so that there are a fixed number of nearest neighbours for each point, depending on the applicability of the RP to a particular type of problem (Marwan 2011). An increase in the size of the threshold correspondingly increases the number of recurrences in the RP. The equation used in the construction of the RP is given by (Marwan *et al.* 2007)

$$R_{i,j} = \Theta(\varepsilon - \|\boldsymbol{x}_i - \boldsymbol{x}_j\|); \quad i, j = 1, 2, \ldots, N_1, \tag{2.2}$$

where Θ is the Heaviside step function (i.e. $\Theta(X) = 0$ if $X < 0$ and $\Theta(X) = 1$ if $X \geqslant 0$), $N_1 = N - (E - 1)T$ is the total number of reconstructed vectors, ε is a predefined threshold and $\|\cdot\|$ is the Euclidean norm. Whenever the phase space trajectory falls within the threshold, it is marked as 1 in the recurrence matrix; otherwise, it is marked as 0. Thus, the RP is a graphical representation of black and white points, where a black point corresponds to $R_{i,j} = 1$ and a white point corresponds to $R_{i,j} = 0$.

We now give the gist of the key measure that we use for the analysis of synchronization in our system. This measure, known as the probability of recurrence ($P(\tau)$) (or also known as the generalized autocorrelation function) shows the probability with which the trajectory returns to the neighbourhood of a given point in the phase space after a time lag τ (Romano *et al.* 2005). The term $P(\tau)$ is given by

$$P(\tau) = \frac{1}{N_1 - \tau} \sum_{i=1}^{N_1 - \tau} \Theta(\varepsilon - \|\boldsymbol{x}_i - \boldsymbol{x}_{i+\tau}\|). \tag{2.3}$$

The recurrence property of a signal can be related to its phase. Whenever the trajectory in the phase space recurs, the phase of a signal can be considered to be increased by 2π (Romano *et al.* 2005). During synchronization, both the phases and the frequencies of the signals from the coupled oscillator system are locked, which, in turn, is reflected in locking of the positions of the peaks corresponding to the two signals in the plots of $P(\tau)$ against the lag. The locking of the height of the peaks in the plot of $P(\tau)$ depends on the correlation between the amplitudes of the interacting signals (Lakshmanan & Senthilkumar 2011). In the case of phase synchronization, the phases of the signals are perfectly locked; nonetheless, their amplitudes may remain uncorrelated. This behaviour is manifested in locking of the positions of the peaks but a mismatch of their heights in the plot of the probability of recurrence. On the other hand, during generalized synchronization, both of the oscillators are bound together by a functional relationship. This translates to the circumstance that if two states in the phase space of one oscillator are close to one another, the states corresponding to the same time instances on the trajectory of the other oscillator are also close to one another (Fujisaka & Yamada 1983). The property of recurrence is able to capture this feature of the proximity of the phase space trajectories. If the two oscillators are in generalized synchronization, their RPs become nearly identical, and hence their plots of probability of recurrence also show identical behaviour (Romano *et al.* 2005; Lakshmanan & Senthilkumar 2011).

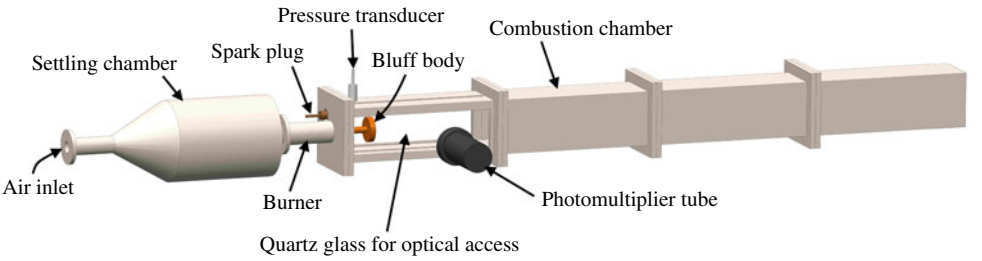

FIGURE 1. (Colour online) A schematic of the turbulent flame combustor. The partially premixed air–fuel mixture is burned in a turbulent flow field inside the combustor. The flame is stabilized using a bluff body located near the dump plane of the combustor.

3. Experimental set-up

The experiments were conducted in a laboratory-scale combustor with a partially premixed turbulent flame, as shown in figure 1. The experimental set-up consists mainly of three parts: (i) a settling chamber, (ii) a burner and (iii) a combustor. The airflow is first passed through the settling chamber, which serves the purpose of reducing the effect of hydrodynamic fluctuations generated inside the combustor on the flow at the air inlet. In the burner, fuel (liquefied petroleum gas, propane 40 % and butane 60 % by volume) is partially mixed with the incoming airflow from the settling chamber at different equivalence ratios. This partially premixed fuel–air mixture then enters the main combustor section. The combustor is a rectangular duct which is 1400 mm long and 90 mm $\times$ 90 mm wide and has a backward-facing step (dump plane) at the inlet. A bluff body, a circular disc of diameter 47 mm and thickness 10 mm, is located at a distance of 4.5 mm from the inlet of the combustor. The bluff body aids in anchoring the flame in the high-velocity turbulent environment of the combustor. The air and fuel flow rates are controlled separately by using mass flow controllers (Alicat Scientific MCR 2000SLPM for air and MCR 100SLPM for fuel; the uncertainty is ± 0.8 % of the measured reading + 0.2 % of the full scale reading) in the system. The fuel flow rate is maintained at a constant value of 25 slpm and the air flow rate is varied from a value of 400 slpm to 940 slpm such that the flow field in the system is turbulent ($Re = 1.09 \times 10^5$ to $Re = 2.12 \times 10^5$) throughout the experiment. The estimated uncertainties in Re are $\pm 1.97 \times 10^3$ to $\pm 2.71 \times 10^3$. The equivalence ratios range from 0.95 ± 0.02 to 0.46 ± 0.01. For the purpose of initial ignition, a spark plug (along with a 11 kV ignition transformer – National Engineering Corporation) fixed at the dump plane is used to ignite the combustible air–fuel mixture. Quartz windows of size 90 mm $\times$ 360 mm, located on both of the sidewalls of the combustor, provide the optical access required for the measurement of heat release rate fluctuations from the flame.

We measure the acoustic pressure fluctuations (p') from the combustor using a piezoelectric transducer (PCB Piezotronics PCB103B02, with a sensitivity of 223.4 mV kPa^{-1} and an uncertainty of ± 0.15 Pa). The pressure transducer is fixed on the top wall near the inlet step of the combustor. This position of the transducer corresponds to a near maximum amplitude of the acoustic pressure in the duct. It is an appropriate location for the measurement of the acoustic pressure in this combustor, as it always remains a pressure antinode for all of the acoustic modes of the duct. The unsteady heat release rate fluctuations ($\dot{q}'$) are captured by using a photomultiplier tube (PMT; Hamamatsu H10722-01). A CH* band-pass filter ($\lambda = 432$ nm and 10 nm

full width at half maximum (FWHM)), which captures the CH^* chemiluminescence intensity from the flame, is used to filter the input to the PMT. The chemiluminescence intensity thus recorded is a measure of the heat release rate from the flame (Ikeda, Kojima & Hashimoto 2002; Guethe *et al.* 2012). The PMT is positioned at a distance of 500 mm normal to the combustor wall near the location of the bluff body. The signals of the pressure fluctuations and the heat release oscillations are acquired for 3 s at a sampling frequency of 10 kHz. A 16-bit analog to digital (NI-6143) card is used for the data acquisition. A frequency resolution of 0.33 Hz is used in the fast Fourier transform calculation. Since our main objective in the present study is to analyse the synchronization characteristics of p' and $\dot{q}'$, we directly use the raw (mean subtracted) voltage signals obtained from the pressure transducer and the PMT throughout our analysis. This further ensures that both p' and $\dot{q}'$ fluctuations are represented in comparable scales of voltage. Welch's average method (Welch 1967) is used to smooth the periodogram of the signals. A Hanning window of 5000 data points with an overlap of 50 % is used in the analysis. This method improves the spectral representation of signals in the waterfall diagram (shown in figure 3) by reducing noise from the estimated power spectra.

4. Results and discussion

We investigate the synchronization behaviour of the acoustic pressure (p') and the heat release rate ($\dot{q}'$) oscillations present in a turbulent combustor, as we vary the mean velocity of the flow ($\bar{u}$). Because a turbulent flow generates sound, there will always be acoustic oscillations in the duct. Further, the measured heat release rate fluctuations incorporate the fluctuations from both chemical kinetics and that induced by the associated flow turbulence present in the system (Shanbhogue, Husain & Lieuwen 2009). As the resulting effects produced from the fluctuations in hydrodynamic and combustion processes in the combustor are difficult to separate, we consider them as a single oscillator, which we call 'turbulent reactive flow'. An increase in $\bar{u}$ results in a decrease in the equivalence ratio of the combustible air–fuel mixture from a value close to stoichiometry ($\phi = 0.98$) to a value of fuel lean condition ($\phi = 0.49$). At lower values of $\bar{u}$ ($\bar{u} = 9.4$ m s^{-1}), we observe low-amplitude aperiodic oscillations in both the acoustic pressure and the heat release rate signals (see figure 2*a*). This state of combustion dynamics is traditionally referred to as combustion noise (Strahle 1978). Recent studies by Nair *et al.* (2013) and Tony *et al.* (2015) have shown that the dynamical features of combustion noise consist of high-dimensional chaos contaminated with white and coloured noise. With further increase in $\bar{u}$ ($\bar{u} = 11.9$ m s^{-1}), we observe the emergence of bursts of periodic oscillations from a background of aperiodic oscillations (figure 2*b*). These bursts appear to occur randomly, with no apparent pattern. Nair *et al.* (2014) referred to this state of combustion dynamics as intermittency. Visual comparison of the acoustic pressure and heat release rate signals (in the inset of figure 2*b*) shows that both of the signals are locked in the burst regions of the periodic oscillations, while unlocked in the relatively silent regions of the aperiodic oscillations.

At sufficiently high values of $\bar{u}$ ($\bar{u} = 13.2$ m s^{-1}), we notice a transition of the combustion dynamics from a state of intermittency to a state of weakly periodic oscillations (figure 2*c*). In this state, we observe wide cycle-to-cycle variation in the amplitude of the pressure signal. This variation in the amplitude of the limit cycle oscillations has been postulated to be due to the forcing exerted by background noise (Lieuwen 2002, 2003*b*; Noiray & Schuermans 2012). With further increase

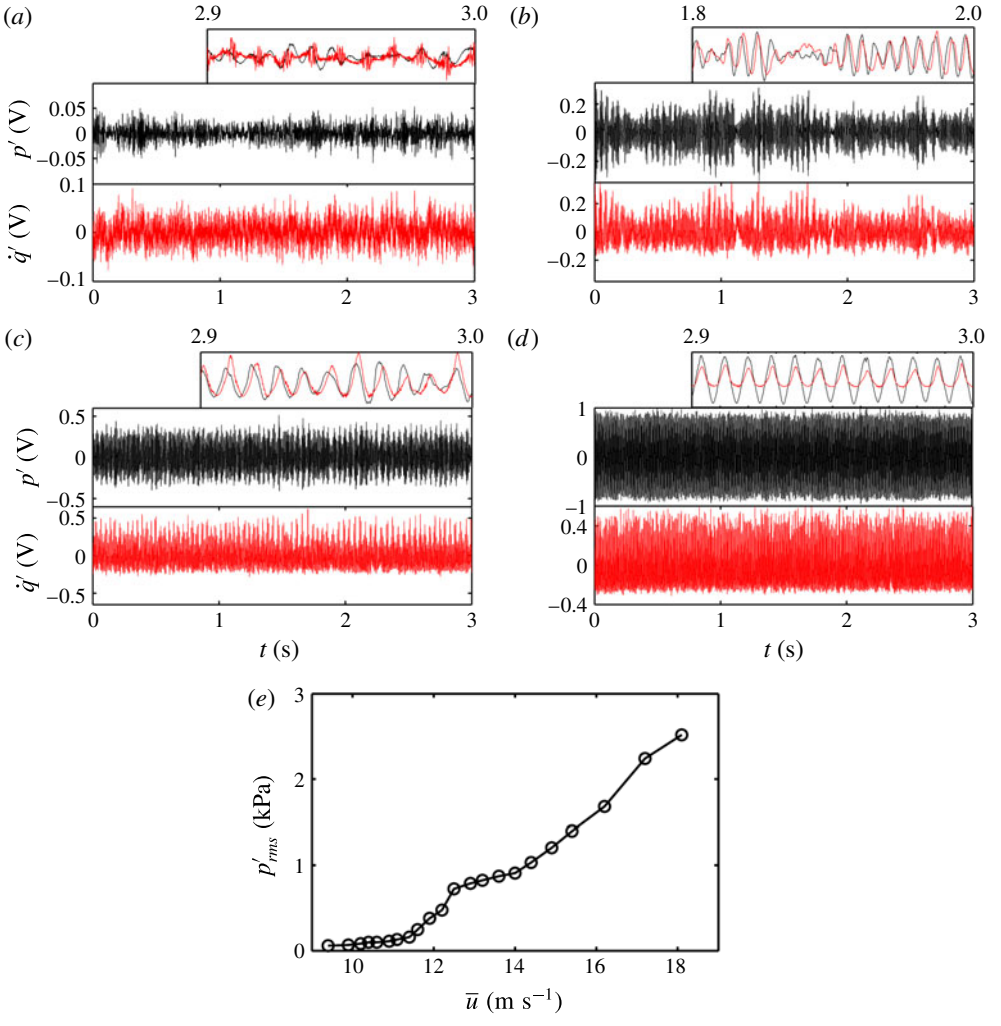

FIGURE 2. (Colour online) (*a–d*) The time series of the acoustic pressure (p' – black colour) and heat release rate ($\dot{q}'$ – red colour) signals obtained from experiments at $\bar{u} = 9.4$ m s^{-1}, $\bar{u} = 11.9$ m s^{-1}, $\bar{u} = 13.2$ m s^{-1} and $\bar{u} = 17.2$ m s^{-1} respectively. Magnified views of the corresponding signals are shown in the insets above each panel. (*a*) A low-amplitude aperiodic state, (*b*) an intermittency, (*c*) a weakly periodic limit cycle state and (*d*) a strongly periodic limit cycle state of oscillations. (*e*) The variation of the root mean square value of the acoustic pressure (p'_{rms}) plotted against the mean velocity of the flow ($\bar{u}$ varies from 9.4 m s^{-1} to 18.1 m s^{-1}).

in $\bar{u}$ ($\bar{u} = 17.2$ m s^{-1}), we observe a transition of the system dynamics to a state of strongly periodic oscillations (figure 2*d*), wherein the amplitude of the pressure oscillations nearly remains the same. Figure 2(*e*) shows the variation of the root mean square value of the acoustic pressure (p'_{rms}) acquired for different values of the mean velocity of the flow ($\bar{u}$). We notice a continuous increase in the amplitude of the pressure oscillations with an increase of $\bar{u}$ in the system. This plot suggests that the growth in the amplitude of the pressure oscillations is not a linear function of $\bar{u}$, as the slope of the plot varies differently in different regions of the system dynamics.

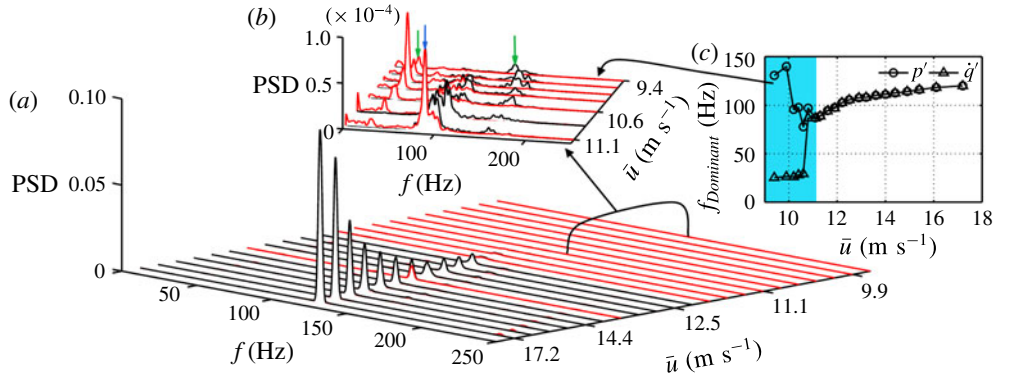

FIGURE 3. (Colour online) (*a*) The variation of the PSD of both p' (black colour) and $\dot{q}'$ (red colour) for a range of $\bar{u}$ from 9.4 m s^{-1} to 17.2 m s^{-1}. (*b*) The magnified view of the PSD for a velocity range from $\bar{u} = 9.4$ m s^{-1} to $\bar{u} = 11.1$ m s^{-1}. (*c*) The variation of the dominant frequency ($f_{Dominant}$) of both p' and $\dot{q}'$ obtained for a range of $\bar{u}$ in the system. The magnified view of the PSD shown in (*b*) is highlighted by a green colour in (*c*). In (*b*), the separate unlocked frequency bands of p' and $\dot{q}'$, obtained for an initial value of $\bar{u} = 9.4$ m s^{-1}, are shown by green arrows, whereas the frequency corresponding to the first onset of frequency lock-in is shown by a blue arrow.

In order to investigate the coupled interaction between the acoustic pressure and the heat release rate oscillations in the system, we plot a waterfall diagram (see figure 3*a*), which demonstrates the variation of the power spectral density (PSD) of the signals obtained at different values of $\bar{u}$. Figure 3(*a*) shows the emergence of sharp dominant peaks in the three-dimensional plot of the PSD for both the acoustic pressure and the heat release rate oscillations at large values of $\bar{u}$. The presence of sharp peaks in the PSD indicates the existence of periodic oscillations in the dynamics of the system. The variation of the dominant frequencies of both the acoustic pressure and heat release rate oscillations, for a range of $\bar{u}$, is plotted in figure 3(*c*). This plot reveals the locking behaviour of the dominant frequencies of both of the signals, which occurs for the first time at $\bar{u} = 11.1$ m s^{-1}. The variation of the dominant frequencies of these signals prior to the locking of frequencies (the highlighted portion of figure 3*c*) is further explored by plotting a zoomed in view of figure 3(*a*) and is shown in figure 3(*b*). At low mean velocities of the flow ($\bar{u} = 9.4$ m s^{-1}), the plots of the PSD for both p' and $\dot{q}'$ show distinct shallow bands of dominant frequencies, around 130.7 Hz for the acoustic pressure signal and around 25.3 Hz for the heat release rate signal (marked by green arrows in figure 3*b*). The dominant peak in the acoustic pressure spectrum corresponds to the fundamental mode of the acoustics in the combustor, which is around 125 Hz (the calculation is based on the assumption of the closed–open geometry of the combustor having a length of 1.4 m, and an approximate value of the speed of sound equal to 700 m s^{-1}). On the other hand, we observe that the dominant frequency corresponding to 25.3 Hz in the heat release rate signal is a consequence of the underlying turbulent hydrodynamic fluctuations present in the reaction zone of the combustor. When the large-scale fluid structures shed from the dump plane impinge on the bluff body and the sidewalls of the combustor, there is a sudden release of heat in the system (observations are based on the high-speed CH* chemiluminescence images of the flame; not shown in this paper). The frequency corresponding to these heat release fluctuations is

close to 25.3 Hz, which indicates that hydrodynamics has a key role to play in the low-frequency oscillations observed in the power spectra of the heat release rate signal.

The existence of different dominant frequencies indicates that these signals are not locked during the stable operation of the combustor. A close inspection of figure 3(*b*) reveals the emergence of a secondary band of frequencies with increasing $\bar{u}$, which is in between the disparate frequency bands that we had for p' and $\dot{q}'$ during aperiodic oscillations. The magnitude of the secondary band frequencies gradually grows with $\bar{u}$; yet, the dominant frequencies of the pressure and heat release rate oscillations in this secondary band still remain different (see the highlighted portion of figure 3*c*). The locking of these dominant frequencies occurs at $\bar{u} = 11.1$ m s^{-1} (around $f_{lock} =$ 86.6 Hz). The presence of distinct frequency peaks for low mean velocities, and the locking of these peaks to a common frequency, which is in between their initial values, indicates the presence of mutual coupling (Pikovsky *et al.* 2003) between these two oscillators of a thermoacoustic system. We further note that such an observation of switching of the dominant frequencies of p' and $\dot{q}'$ to a secondary frequency band, which is sufficiently away from the natural acoustic mode of the duct, is different from the problem of forced flame response, wherein the low frequency associated with heat release rate fluctuations is damped and a single peak arises at the forcing frequency. However, whether the phenomenon we observe can be termed as merging or adjustment of frequencies needs to be clarified through further studies.

Frequency analysis of the acoustic pressure and heat release rate oscillations (figure 3*c*) reveals an important feature of the locking of dominant frequencies of these signals in our system: it occurs in the intermittency state ($\bar{u} = 11.1$ m s^{-1}), long before the onset of limit cycle oscillations ($\bar{u} = 13.2$ m s^{-1}) in the system. Possible physical mechanisms that bring about the locking of frequencies of p' and $\dot{q}'$ during the onset of intermittency could be the locking of hydrodynamic and acoustic oscillators during periodic epochs of the intermittent oscillations. To further explore this proposition, we refer to the study performed by Unni & Sujith (2015), where they described the behaviour of the flame during intermittency. They observed that during the periodic segments of intermittency, ring vortices are periodically shed from the dump plane and convected downstream along the outer shear layer. This causes periodic fluctuations in the flame surface area, and when the shed vortex impinges on the obstacles (the bluff body and the sidewalls), we correspondingly have periodic heat release in the system. On the other hand, during aperiodic epochs of the oscillations, this periodic shedding of vortices ceases, and the tip of the flame exhibits oscillations in an aperiodic manner. We further need to keep in mind that the vortex shedding itself might be influenced by the acoustics and combustion dynamics in the system. Hence, all three of these processes are likely to play a role in the mutual synchronization during the periodic epochs of intermittency. The dominant frequencies of the p' and $\dot{q}'$ oscillators remain locked as the system dynamics changes from intermittency ($\bar{u} = 11.1$ m s^{-1}) to limit cycle oscillations ($\bar{u} = 17.2$ m s^{-1}). During the onset of limit cycle oscillations, we observe periodic shedding of large-scale vortices, and hence a periodic heat release rate, during every acoustic cycle. We further notice that this locked-in frequency of the signals continuously increases with $\bar{u}$ until the final state (see the non-highlighted portion of figure 3*c*).

To ascertain the synchronization behaviour of the acoustic pressure and heat release rate oscillations, we use a statistical measure of synchronization based on the RPs. This is the same measure as we described previously in § 2.2: the probability of recurrence ($P(\tau)$). We compute $P(\tau)$ for p' and $\dot{q}'$, and then compare the coincidence

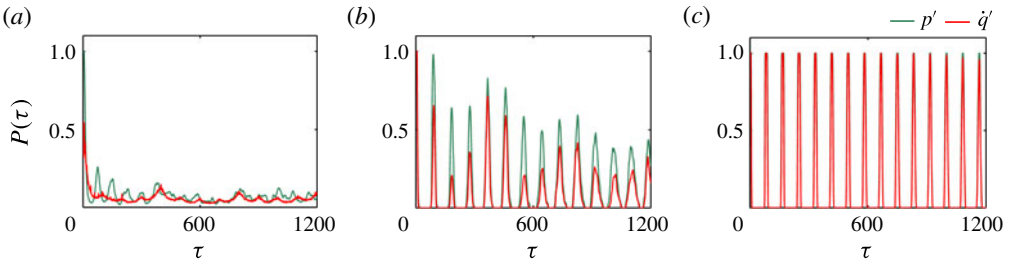

FIGURE 4. (Colour online) Plots of probability of recurrence ($P(\tau)$) of a phase space trajectory at different values of the time lag (τ) for p' (green colour) and $\dot{q}'$ (red colour). (*a–c*) $P(\tau)$ corresponding to three states of synchronization, namely desynchronization (aperiodic oscillations), phase synchronization (periodic oscillations) and generalized synchronization (periodic oscillations), obtained at $\bar{u} = 9.4$ m s^{-1}, $\bar{u} = 13.2$ m s^{-1} and $\bar{u} = 17.2$ m s^{-1} respectively. The parameters used are embedding dimension = 12, time delay = 2 ms and recurrence threshold = 25 % of the maximum size of the attractor. The data set contains 3000 points (shown for 1200 points).

of the peaks of $P(\tau)$ obtained from these signals in order to analyse the synchrony between them (Romano *et al.* 2005).

Figure 4(*a*) shows a plot of $P(\tau)$ as a function of the time lag τ, for both the acoustic pressure and the heat release rate signals, obtained during the aperiodic state (as shown in figure 2*a*). We see from the figure that there is no correspondence between the peaks of $P(\tau)$ of these signals. This confirms that the two oscillators are not in synchrony. On the other hand, when the system dynamics undergoes a transition to limit cycle oscillations (see figure 2*c*,*d*), we see a perfect locking of the positions of the peaks of $P(\tau)$ of both of the signals, as shown in figure 4(*b*,*c*). The locking of the positions of the peaks confirms the synchronization between acoustic pressure and heat release rate oscillations. Furthermore, the absence of exact locking of the heights of these peaks in figure 4(*b*) indicates that we have phase synchronization (PS) in the system (Romano *et al.* 2005). Figure 4(*c*) reveals the perfect coincidence of the height as well as the position of the peaks of the probability of recurrence obtained from the acoustic pressure and the heat release rate oscillations, suggesting the presence of generalized synchronization (GS) in the system (Romano *et al.* 2005). Previous studies on synchronization have reported chaotic oscillators synchronizing in the chaotic state (Boccaletti *et al.* 2002) or periodic oscillators synchronizing in the periodic state (Blekhman *et al.* 1995). However, in our system, chaotic oscillators transition to the periodic state as they synchronize. This makes the study of such a synchronization transition quite interesting.

We therefore analyse the synchronization behaviour of acoustic pressure and heat release rate oscillators during intermittency (see figure 5), as this is the intermediate state of the transition. Since the intermittent oscillations consist of alternating occurrences of high-amplitude periodic and low-amplitude aperiodic oscillations, we plot $P(\tau)$ for short windows of the periodic (figure 5*b*) and aperiodic (figure 5*c*) regions of the signals. The plot of $P(\tau)$ for a periodic window (figure 5*b*), corresponding to both p' and $\dot{q}'$, shows locking of the positions of the peaks without locking of their heights, which confirms the phase synchronization of the two signals during the periodic epoch. On doing the same for the aperiodic region, we see a mismatch in the locations as well as the heights of the peaks; this depicts the desynchronized behaviour during the aperiodic phase. The alternate switching of the

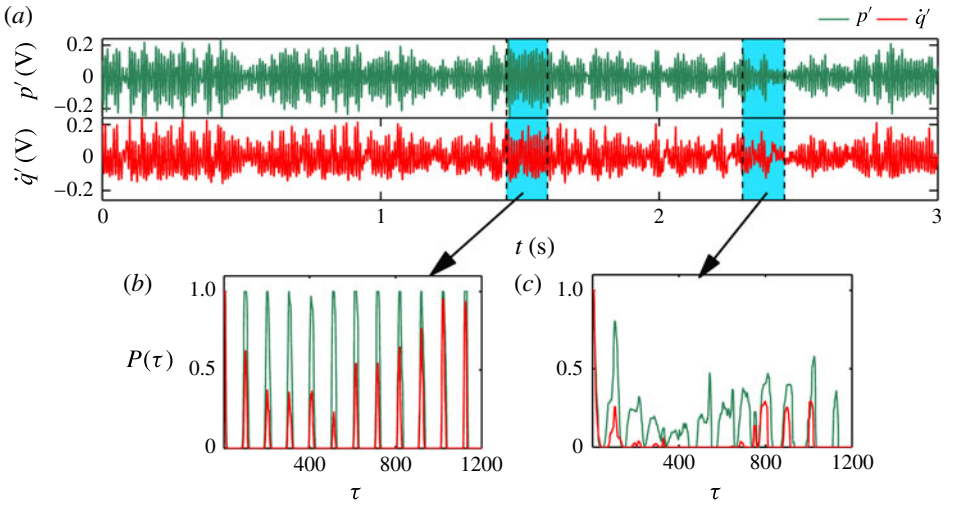

FIGURE 5. (Colour online) (*a*) Plots of time series of p' (green colour) and $\dot{q}'$ (red colour) acquired during the intermittency state at $\bar{u} = 11.6$ m s^{-1}. (*b*,*c*) Plots of $P(\tau)$ shown for periodic and aperiodic regions of both p' and $\dot{q}'$ respectively. The parameters used in plotting (*b*,*c*) are embedding dimension = 12, time delay = 2 ms and recurrence threshold = 25 % of the maximum size of the attractor. The data set contains 3000 points (shown for 1200 points).

coupled oscillators between synchronized and desynchronized behaviour describes the property of intermittent synchronization in the system. Moreover, since the two oscillators in our system are phase synchronized in the periodic region and desynchronized in the aperiodic region, such a state of the system is referred to as intermittent phase synchronization (IPS). This state shows that the oscillators in our system gradually change their underlying dynamics from aperiodic to periodic as they synchronize. Recently, Mondal, Unni & Sujith (2017) investigated the spatio-temporal synchronization behaviour of the local heat release rate in the flame with the global acoustic field of the duct. During intermittency, their study demonstrated the coexistence of patches of both synchronized periodic oscillations and desynchronized aperiodic oscillations in the reaction zone. Furthermore, these patterns of spatial synchrony and desynchrony interchanged as the flow convected downstream, which they referred to as a breathing chimera-like state. Therefore, IPS is arguably an apt intermediate state that we observe during the transition of combustion dynamics from a state of completely desynchronized oscillations to a state of perfectly phase synchronized oscillations. Thus, it is evident from figures 4 and 5 that in the turbulent flame combustor examined in the present study, the desynchronized oscillations pave the way to PS through IPS, and subsequently to GS with an increase in the mean velocity of the flow ($\bar{u}$).

As discussed earlier, the unstable operation of a turbulent combustor has been traditionally perceived in terms of limit cycle oscillations (Lieuwen 2002). We, however, observe two different types of limit cycle in our system, which exhibit different dynamical characteristics. We call them weakly correlated (PS) and strongly correlated (GS) limit cycle oscillations. In order to identify the distinguishing features of these two states, we compare the temporal variation in instantaneous phase difference (relative phase) between the acoustic pressure and the heat release rate

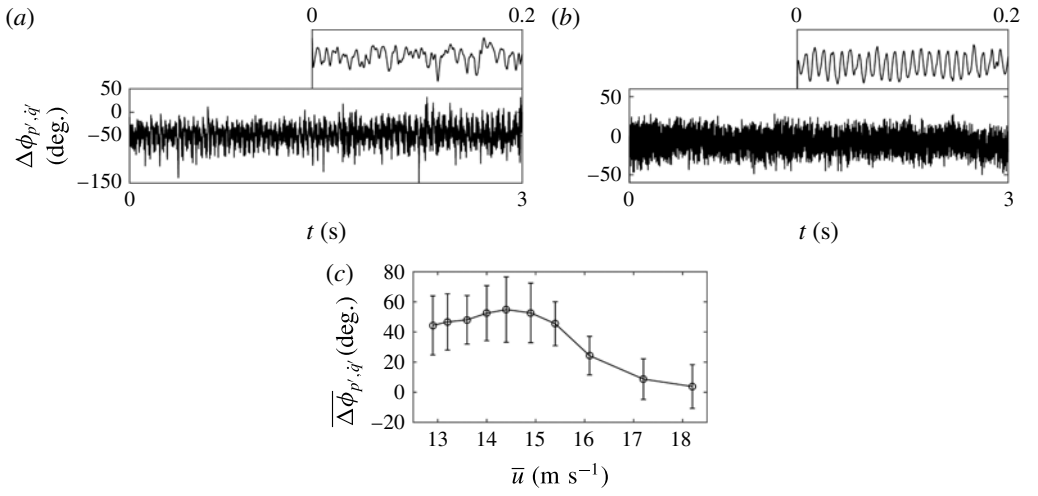

FIGURE 6. (a,b) The temporal variation of the relative phase ($\Delta\phi_{p',\dot{q}'}$) between p' and $\dot{q}'$ calculated using an analytical signal approach based on the Hilbert transform. (a) The PS ($\bar{u} = 13.2$ m s^{-1}) and (b) the GS ($\bar{u} = 17.2$ m s^{-1}) state of oscillations. (c) A plot depicting the variation of the mean value of the relative phase ($\overline{\Delta\phi}_{p',\dot{q}'}$) with the mean velocities of the flow observed during the PS and GS states.

oscillations. The instantaneous phases of these signals are calculated using the Hilbert transform (explained in § 2.1). Figures 6(a) and 6(b) show the relative phase plots ($\Delta\phi_{p',\dot{q}'}$) of these signals obtained during PS and GS states respectively. The fluctuation of the relative phase around a constant phase shift (as shown in figure 6a,b) suggests synchronization of the signals of the coupled oscillator system (Pikovsky *et al.* 2003). The enlarged view of the relative phase for the PS state shows a noisy behaviour (figure 6a), while that for the GS state shows an apparently periodic behaviour (figure 6b). In figure 6(c), we plot the temporal mean value of the relative phase ($\overline{\Delta\phi}_{p',\dot{q}'}$), in the interval $-180°$ to $180°$, versus different values of the mean velocities of the flow. The plot shows the velocity range corresponding to PS and GS states alone. During the PS state, we notice that the mean value of the relative phase remains close to 50°, whereas during the GS state (figure 6b), it approaches a value closer to zero degrees (refer to figure 6c). Thus, we observe a reduction in the mean phase angle between the acoustic pressure and the heat release rate fluctuations as the system dynamics transitions from the PS to the GS state.

It should be recalled that when two oscillators are in GS, there exists a functional relation between the dynamics of these oscillators (Rulkov *et al.* 1995). Say, for example, that we have two non-identical oscillators, namely $X(t)$ and $Y(t)$. When these oscillators are in the state of GS, there exists a functional relationship between them, which can be expressed as $Y(t) = \Phi(X(t))$. This means that the response of $Y(t)$ can be uniquely determined from $X(t)$ if the functional form of their relation is known (Pyragas 1998). However, the determination of the exact functional form for experimental signals is not straightforward.

In our system, we can obtain an approximate functional relation between the acoustic pressure (p') and the unsteady heat release rate ($\dot{q}'$) during the GS state, using the knowledge obtained from experiments. During the GS state (see figure 7a), visual inspection of the acoustic pressure signal hints at the features of a sinusoidal

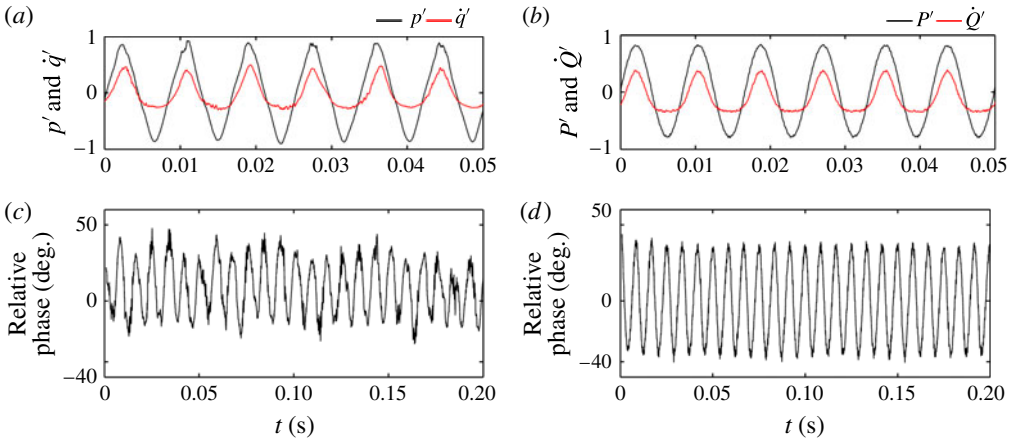

FIGURE 7. (Colour online) (*a*) A portion of the time series of p' (black colour) and $\dot{q}'$ (red colour) obtained from experiments during the GS state ($\bar{u} = 17.2$ m s^{-1}). (*b*) A portion of the signal obtained from an assumed functional form for both acoustic pressure (P' – black colour) and heat release rate ($\dot{Q}'$ – red colour) oscillations. (*c*,*d*) The temporal variation of the relative phase obtained from the Hilbert transform for the signals shown in (*a*) and (*b*) respectively.

function, whereas the heat release rate signal shows the features of a spiky signal. By saying spiky, we mean that the signal is relatively flat for some time, then rises up, decays and becomes flat again. The behaviour of these signals can then be qualitatively mimicked by the following equations:

$$P' = [a_1 + n_{p1}(t)] * \sin[\omega t \pm \emptyset_1 + n_{p2}(t)] \tag{4.1}$$

and

$$\dot{Q}' = [a_2 + n_{q1}(t)] * \sin[\omega t + a_3 \sin(\omega t \pm \emptyset_2) + n_{q2}(t)], \tag{4.2}$$

where P' and $\dot{Q}'$ are the assumed functional forms of p' and $\dot{q}'$, ω is the angular frequency of the signals, a_1, a_2 and a_3 are constants and $\emptyset_1$ and $\emptyset_2$ are the initial phases of P' and $\dot{Q}'$ respectively. Here, n_{p1}, n_{p2}, n_{q1} and n_{q2} are Gaussian white noise terms added to the amplitude and phase parts of the signals.

The values of the constants in the assumed functional forms of P' and $\dot{Q}'$ are derived from the statistical properties of the corresponding p' and $\dot{q}'$ signals obtained from experiments. This is to ensure an approximate fit between the data generated from numerical results and the signals obtained from experiments.

The relative phase between the two signals can then be expressed as

$$\Delta\emptyset = \{\omega t + a_3 \sin(\omega t \pm \emptyset_2)\} - \{\omega t \pm \emptyset_1\} + G(t) = a_3 \sin(\omega t \pm \emptyset_2) \pm \emptyset_1 + G(t), \tag{4.3}$$

where $G(t)$ is the phase noise present in the relative phase of both P' and $\dot{Q}'$.

The parameters selected in plotting figure 7(*b*) are $a_1 = 0.8$, $a_2 = 0.35$, $a_3 = 0.7$, $\omega = 120.2$ Hz, $\emptyset_1 = 0$ rad and $\emptyset_2 = \pi/2$ rad, and the strength of noise is 0.05.

Figure 7(*b*) qualitatively simulates the features of the acoustic pressure and the heat release rate oscillations observed in experiments during the GS state (figure 7*a*).

The plot of the relative phase between the two signals obtained from the experiments (figure 7*c*) is qualitatively captured by the proposed functional form for these signals (figure 7*d*). These analogies between the experimental results and the assumed functional relation are completely drawn from the characteristics of the acoustic pressure and the heat release oscillations observed during the GS state. In reality, the functional relationship may be considerably more complicated, involving different combinations of sine and cosine functions along with inherent turbulent fluctuations present in the combustion system. Identification of the exact functional form of these signals is difficult, mainly because the complex interaction between acoustic pressure and heat release rate oscillations is still not completely known.

We now try to elucidate the possible physical reason for having separate PS and GS states in our turbulent flame combustor. Towards this purpose, we calculate the amplitude difference (figure 8*a*) and the time difference (figure 8*b*) between the consecutive cycle peaks of the acoustic pressure and the heat release rate oscillations respectively, and subsequently compare them for the PS (figure 8*c*,*d*) and GS (figure 8*e*,*f*) states. The time at which $\dot{q}'$ reaches a local maximum is referred to as a kicking time (figure 8*b*). The reason for using such a terminology is to relate it to the kicked oscillator model that we propose in § 5. The term kick refers to the release of heat in a very short time span when the shed vortex from the dump plane impinges on the bluff body. This sudden generation of heat leads to the spiky behaviour in $\dot{q}'$. Figures 8(*d*) and 8(*f*) show the difference in the impingement time (i.e. the kicking time) of two consecutive vortices (normalized by the period, $T = 1/f_{Dominant}$) obtained during the PS and GS states respectively. We observe a wide variation in the kicking times of the vortex during PS compared with what is seen during GS.

The variation in the kicking times is possibly reflected in the irregular nature of the amplitudes of the acoustic pressure oscillations observed during PS. Figures 8(*c*) and 8(*e*) show plots of the amplitude difference between consecutive cycles of the acoustic pressure (p') signal, normalized by the global maximum (p'_{max}) of the respective signal, for the PS and GS states respectively. We notice that the cycle-to-cycle variation in the amplitude of p' is comparatively much larger during the PS state than that during the GS state. The consequence of such cycle-to-cycle variation in the kicking times as well as in the amplitudes of the signals observed during PS and GS is further investigated by plotting a linear measure of correlation between p' and $\dot{q}'$ for the whole range of $\bar{u}$ used in this study (see figure 8*g*). The cross-correlation coefficient (r) (or Pearson's coefficient) is a measure of the strength of the linear relation between the two signals. It further helps in determining the synchronization of amplitudes of the signals obtained from a coupled oscillator system (Gonzalez-Miranda 2002; Bove *et al.* 2004), and is given by the following equation:

$$r = \frac{n\sum_{i=1}^{n} x_i y_i - \sum_{i=1}^{n} x_i \sum_{i=1}^{n} y_i}{\left\{\left(n\sum_{i=1}^{n} x_i^2 - \left(\sum_{i=1}^{n} x_i\right)^2\right)\left(n\sum_{i=1}^{n} y_i^2 - \left(\sum_{i=1}^{n} y_i\right)^2\right)\right\}^{0.5}}, \tag{4.4}$$

where x_i and y_i are the samples of the bivariate data obtained from the experiments and n is the total number of samples in the signal.

The values of r range from -1 to $+1$; $r = -1$ corresponds to strong negative correlation and $r = 1$ corresponds to strong positive correlation between the signals.

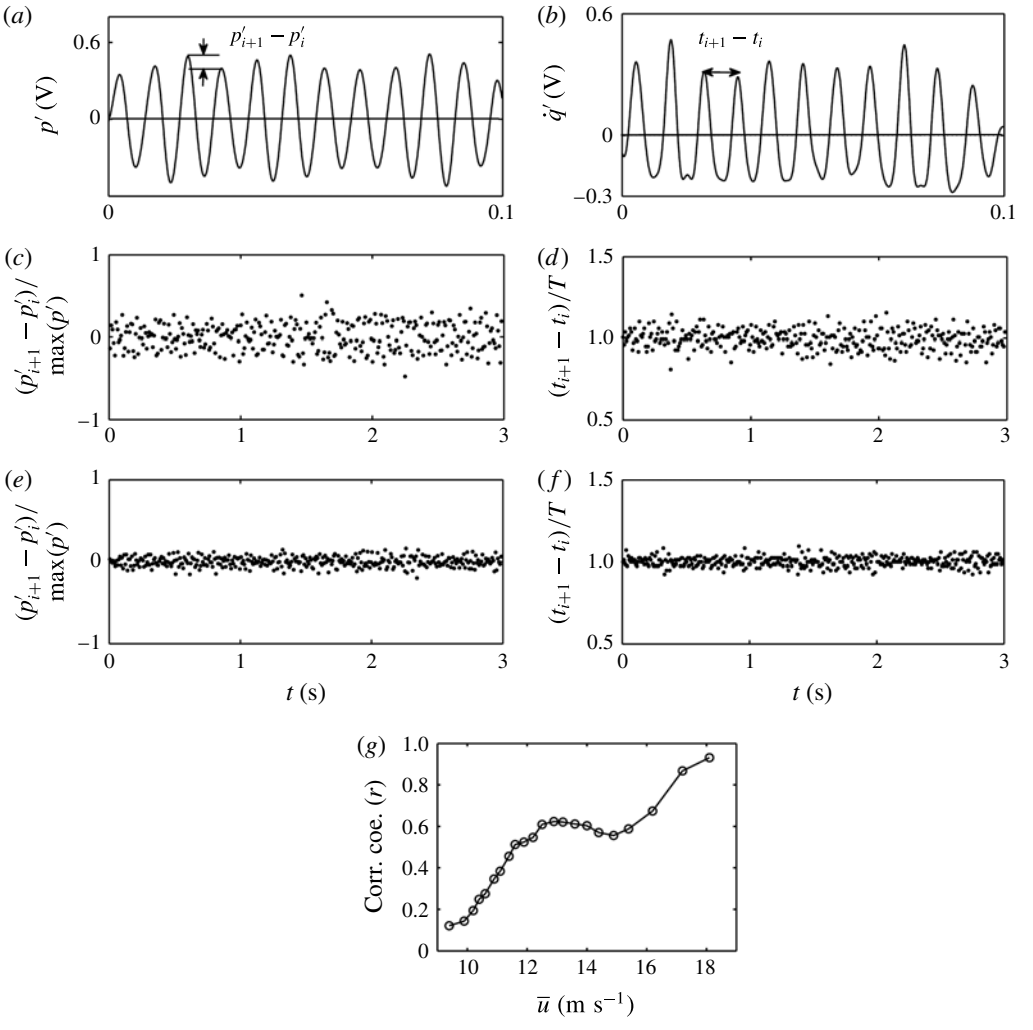

FIGURE 8. The portion of (*a*) acoustic pressure and (*b*) heat release rate oscillations depicting the computation procedure for the amplitude difference and the kicking times respectively. (*c*,*e*) The temporal variation of the amplitude difference (normalized by signal global maxima) between consecutive peaks of the acoustic pressure oscillations obtained for PS and GS states respectively. (*d*,*f*) The temporal variation of the time difference (normalized by the signal period $T = 1/f_{Dominant}$) between the consecutive peaks of the heat release rate oscillations, referred to as kicking times, obtained for PS and GS states respectively. The PS state corresponds to $\bar{u} = 13.2$ m s^{-1} and the GS state corresponds to $\bar{u} = 17.2$ m s^{-1}. (*g*) The variation of the cross-correlation coefficient (r) between p' and $\dot{q}'$ with different values of the mean velocity of the flow ($\bar{u}$).

The value $r = 0$ indicates zero linear correlation between the signals. In our system, we observe values of r greater than zero, suggesting the presence of a positive correlation between the acoustic pressure and heat release rate oscillations (figure 8*g*). We notice an increase in the value of the linear correlation as the system dynamics transitions from combustion noise to a final state of limit cycle oscillation. During PS, the weak correlation of the oscillators is reflected in relatively low values of r,

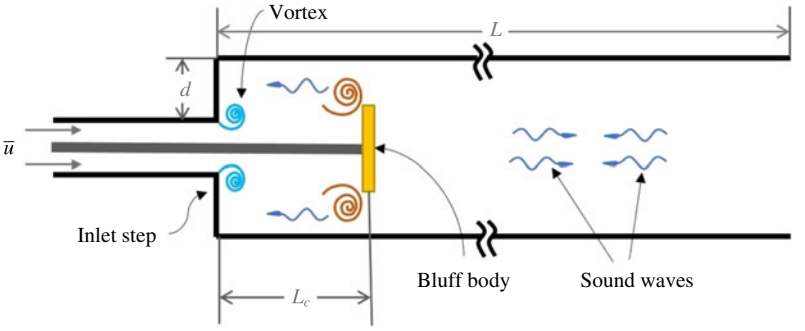

FIGURE 9. (Colour online) Schematic of the combustor model. The inlet end contains a step of height d from which vortices are shed. These shed vortices carry reactant mixture at a fraction of the mean velocity of the flow ($\bar{u}$). The reactant mixture burns when these vortices impinge on the bluff body, located at a distance L_c from the inlet. The acoustic waves generated as a result of this burning affect the vortex shedding, and thus establish a closed loop interaction between hydrodynamic, combustion and acoustic processes.

which are around 0.5–0.6. Although the amplitude of the acoustic pressure oscillations shows a significant increase for all of the values of $\bar{u}$ ($\bar{u} = 12.9$ m s^{-1}–15.4 m s^{-1}) during PS (figure 2*e*), the value of r shows a marginal variation during this state (figure 8*g*). The transition from PS to GS results in an increase in the value of r from a value close to 0.5 to a value close to 1. Thus, the oscillators in GS ($\bar{u} = 16.1$ m s^{-1}–18.5 m s^{-1}) in our system are very strongly correlated. Changes in the behaviour of both the kicking time and the cycle-to-cycle amplitude variation have a major impact on the linear correlation during the transition from the PS to the GS state.

5. Model

Lastly, we introduce a phenomenological model that qualitatively captures the experimental results. The model takes into account the three important phenomena vital to the problem at hand – hydrodynamics, combustion of reactants and propagation of sound waves in the duct (see figure 9). For a set of values of the control parameter, the interactions between these subsystems intertwine in a manner that gives rise to self-sustained synchronized oscillations in a thermoacoustic system. Matveev & Culick (2003) developed a reduced-order model that captures interactions between the vortex shedding, acoustic field and combustion processes of such systems. They modelled the interaction of the heat release rate with the acoustic field as a kicked oscillator system, where the vortices that impinge on the bluff body impulsively force the acoustic field. Their model was able to capture the stable and unstable operation of the combustor; however, it did not show intermittency prior to thermoacoustic instability. Nair & Sujith (2015) extended Matveev's model to capture the state of intermittency in the system dynamics. In order to capture the intermittent dynamics, they added a stochastic noise term in the convection velocity of the vortex. Seshadri, Nair & Sujith (2016) used a deterministic approach to capture all of the dynamical states such as combustion noise, intermittency and limit cycle oscillations of a thermoacoustic system. They suggested that the feedback due to the acoustic waves, generated as a result of the instantaneous release of heat at the bluff body, affects the vortex shedding process at the dump plane of the combustor.

Here, we consider a simplified configuration of the experimental system for construction of the model (see figure 9) while retaining the key geometrical features of the real turbulent combustion system. The combustor is of length L, with a step at the inlet of height d. The combustion of the reactants is assumed to be localized at a distance L_c from the inlet end (Matveev & Culick 2003). Vortices containing unburnt reactants are formed at the inlet end, which is due to the build-up of circulation at the step. This process of build-up of circulation (Γ) is described by (5.1), where $u_{sep} = \bar{u} + u'(L_s, t)$ is the velocity at the step, $\bar{u}$ is the mean velocity, $u'(L_s, t)$ is the acoustic velocity at the step and p'_{L_c} is the acoustic pressure at the point of combustion (i.e. at L_c),

$$\frac{\mathrm{d}\Gamma}{\mathrm{d}t} = \frac{u_{sep}^2}{2} + k\sum_j p'_{L_c}(t_j)\delta(t - t_j - \tau_a) + \sigma_1 N(0, 1). \tag{5.1}$$

Here, t_j is the time when the jth vortex reaches the combustion location, k is a proportionality factor (Seshadri *et al.* 2016), τ_a is the time taken by the acoustic wave to reach the inlet from L_c and σ_1 indicates the intensity of the Gaussian white noise $N(0, 1)$. The second term in the above equation describes the delayed feedback of acoustics on the vortex shedding process at the step. The form of (5.1) is similar to that proposed by Seshadri *et al.* (2016), except that we have additionally incorporated a noise term; we will soon explain the reason for this.

When the circulation exceeds a critical value ($\Gamma_{cr} = \Gamma_o u_{sep}$), a vortex is shed from the step, and the circulation is reset to zero (Matveev & Culick 2003). Here, Γ_o is given as $d/(2S_t)$, where S_t is the Strouhal number (Matveev & Culick 2003). In the experiments, the inlet is not a perfectly closed end, as opposed to what has been assumed in the previous models (note that for a perfectly closed end, $u_{sep} = \bar{u}$). Further, the turbulence of the flow at the inlet affects the circulation building up at the step. For this reason, we incorporate a noise term, which accounts for the variation in the velocity at the step (which appears in (5.1)), and correspondingly obtain Γ_{cr} as $\Gamma_{cr} = \Gamma_o u_{sep} + \sigma_2 N(0, 1)$. We note that the source of the noise is same for both $\mathrm{d}\Gamma/\mathrm{d}t$ and Γ_{cr}, but it affects them with strengths σ_1 and σ_2 respectively. The repeated process of increase in the value of the circulation up to a critical value and its subsequent fall to zero depicts the oscillatory behaviour of the circulation. The vortex shed from the inlet convects downstream at a fraction of the mean velocity, and this is captured by (5.2) (Matveev & Culick 2003),

$$\frac{\mathrm{d}x_j}{\mathrm{d}t} = \alpha\bar{u} + u'(x, t). \tag{5.2}$$

Here, α gives the fraction of $\bar{u}$ with which the vortex is transported.

When these vortices reach the location of combustion (L_c), a localized and instantaneous burning of the reactants in the vortex occurs, and, corresponding to this event, the generated heat release rate ($\dot{q}'$) is modelled as (Matveev & Culick 2003)

$$\dot{q}' = \beta\sum_j \Gamma_j\delta(x - L_c)\delta(t - t_j). \tag{5.3}$$

The heat release rate fluctuations ($\dot{q}'$) affect the acoustic oscillations (p' and u') present in the duct at time instants t_j, when the reactants in the vortices burn.

The acoustic pressure (p') and velocity (u') in the duct are decomposed into a product of time-varying components (η_n, $\dot{\eta}_n$) with the natural spatial modes (M) of the duct as follows (Zinn & Lores 1971; Seshadri *et al.* 2016):

$$p'/\bar{p} = \sum_{n=1}^{M} \frac{\dot{\eta}_n(t)}{\omega_n} \cos(k_n x) \quad \text{and} \quad u'/(\bar{p}/\bar{\rho}c) = \sum_{n=1}^{M} \eta_n(t) \sin(k_n x), \tag{5.4a,b}$$

where $k_n = \omega_n/c$.

Using the energy conservation equation, we obtain an oscillatory equation for the coefficients of the natural modes (η_n, $\dot{\eta}_n$),

$$\ddot{\eta}_n + \zeta_n \dot{\eta}_n + \omega_n^2 \eta_n = b\omega_n \cos(k_n L_c) \sum_j \Gamma_j \delta(t - t_j), \tag{5.5}$$

where b is a proportionality constant. Here, the damping term has been artificially introduced, and the damping coefficient (ζ_n) is modelled as $\zeta_n = (2n-1)^2 \zeta_1$ (Nair & Sujith 2015; Seshadri *et al.* 2016).

When the acoustic oscillations are excited, the sound waves travel upstream and affect the circulation build-up at the step, after a time delay of τ_a (Seshadri *et al.* 2016), which is evident from (5.1). This dependence of the circulation on the acoustic field closes the feedback loop of interaction between the acoustic oscillations in the duct, the vortex shedding and the combustion processes. We note that the heat release rate ($\dot{q}'$) in the system can be related to the circulation (Γ) at the step as the shedding of a vortex is controlled by (5.1). Consequently, we study the synchronization of the acoustic pressure oscillations (p') and the circulation (Γ) obtained from the model. We remark that the acoustic oscillator described in the model is not a self-sustained oscillator and hence is not an ideal candidate for the synchronization study. The turbulent flow in the duct contributes to the production of sound in the actual system, and thus the acoustic variables would not decay even in the absence of a heat release rate. This can be captured in this model by adding a noise term to the evolution equation governing the acoustic modes, or through a more detailed modelling of the system incorporating turbulent flow. We nevertheless stick to the current model for studying the synchronization behaviour of acoustics and circulation, as we are only trying to compare a phenomenological model with the experiments.

Further, given that the model proposed by Seshadri *et al.* (2016) captures the transition from combustion noise to thermoacoustic instability via the intermittency route, a question arises as to what prompted us to incorporate noise into the system. We here present the motivating reason for such a modification. We observed that the model by Seshadri *et al.* (2016) showed desynchronized oscillations, IPS and GS, but we could not observe the state of PS (note that, in the absence of noise, the empirical parameters need to be appropriately chosen to obtain the intermittency route to thermoacoustic instability). In other words, the subsystems in the previous model are very strongly correlated during the limit cycle oscillations (thus giving rise to GS but not PS), and, therefore, some aspect that induces a weakly correlated limit cycle is being overlooked. A plausible reason for not observing PS in the previous model, as we have explained above, is that the inlet end of the duct is not perfectly closed (as opposed to what is assumed in that model), and the turbulence in the flow gives rise to small fluctuations that affect the circulation build-up at the inlet step. This is not captured in the model presented by Seshadri *et al.* (2016). We incorporate these fluctuations as noise in the current model, paving the way to (5.1). We note that our

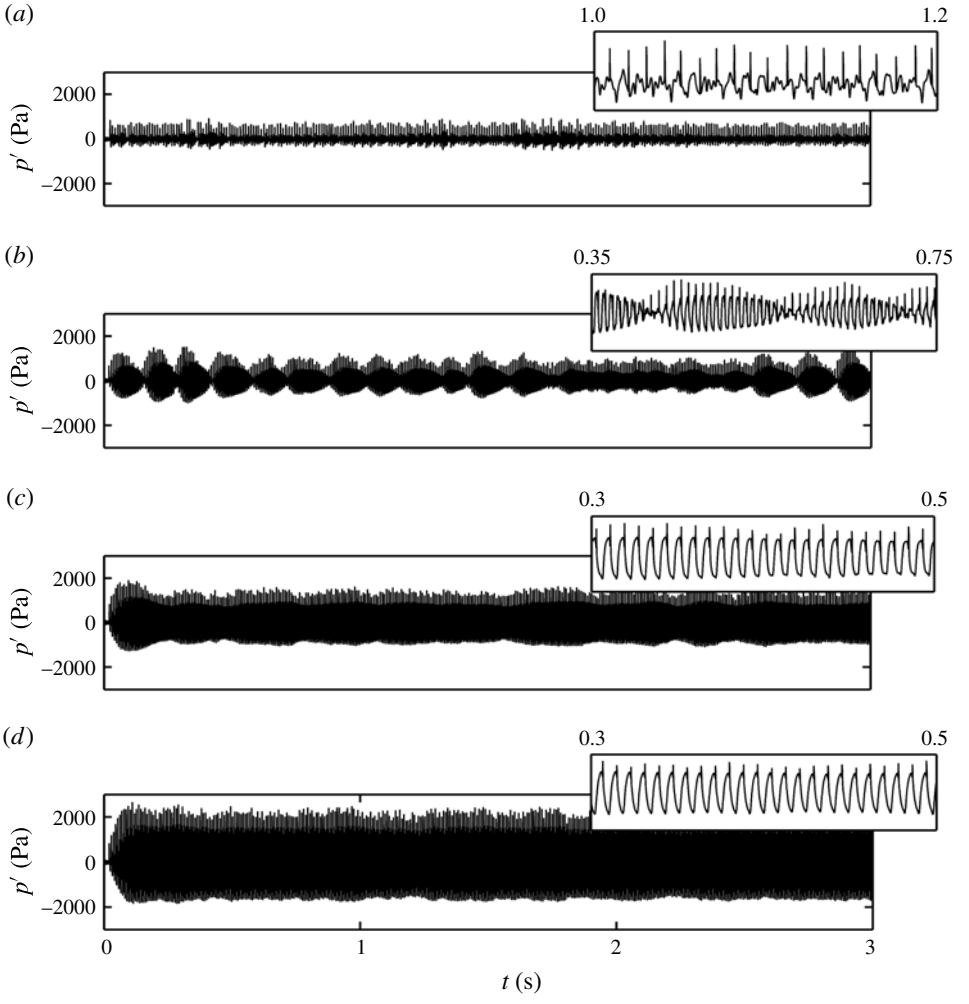

FIGURE 10. The time series of the acoustic pressure (p') obtained from the model showing (*a*) low-amplitude aperiodic oscillations at $\bar{u} = 9.2$ m s^{-1}, (*b*) an intermittency signal at $\bar{u} = 10.2$ m s^{-1}, (*c*) low-amplitude periodic oscillations at $\bar{u} = 10.41$ m s^{-1} and (*d*) high-amplitude periodic oscillations at $\bar{u} = 10.6$ m s^{-1}. (*a*) The desynchronized state, (*b*) the IPS state, (*c*) the PS state and (*d*) the GS state of oscillations is observed when the acoustic pressure (p') is compared with the circulation (Γ) at the step. The data were acquired for 3 s and then undersampled to a frequency of 10 kHz.

intention is to effect minimal changes to the previous model so that a qualitative match with the experimental observation is obtained.

We used the Runge–Kutta method of order 4 for performing the integration of the deterministic part of the above equations, while the Euler–Maruyama scheme was employed in integrating the stochastic part. The values of the parameters used in the computations are $\mathrm{d}t = 10^{-5}$, $\alpha = 0.53$, $\gamma = 1.4$, $\zeta_1 = 29$ s^{-1}, $L_c = 0.045$ m, $L = 1.4$ m, $d = 0.025$ m, $c = 700$ m s^{-1}, $\bar{p} = 101\,325$ Pa, $M = 10$, $S_t = 0.145$ (i.e. $\Gamma_0 = 0.086$), $k = 12.9 + 6.2 * S^*(\bar{u} - 9.4)$, $b = 0.003$, $\sigma_1 = 0.017$ and $\sigma_2 = 0.0937$, where S^* is the step function.

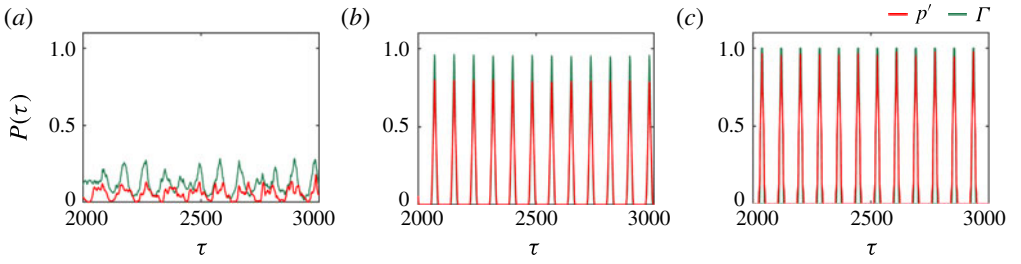

FIGURE 11. (Colour online) (*a–c*) The probability of recurrence ($P(\tau)$) of the phase space trajectory for the signals (p' – green colour; Γ – red colour) obtained from the numerical model at $\bar{u} = 9.2$ m s^{-1}, $\bar{u} = 10.41$ m s^{-1} and $\bar{u} = 10.6$ m s^{-1} respectively. (*a*) The desynchronized state, (*b*) a PS state and (*c*) a GS state of oscillations. The parameters used in plotting are embedding dimension = 12, time delay = 2 ms and recurrence threshold = 20 % of the maximum size of the attractor. The data window contains 4000 points (shown for 1000 points).

Figure 10 shows a plot of the time series of the acoustic pressure obtained at different states of synchronization from the theoretical model. At low values of the mean velocities of the flow ($\bar{u}$), we notice low-amplitude aperiodic oscillations in the system, as shown in figure 10(*a*). With further increase in $\bar{u}$, we observe the emergence of bursts of large-amplitude periodic oscillations from the background of low-amplitude aperiodic oscillations in the system (see figure 10*b*). Since this type of oscillation consists of alternate occurrence of both periodic and aperiodic oscillations, it corresponds to the state of intermittency. At sufficiently large values of $\bar{u}$, the system dynamics transitions to a state of low-amplitude limit cycle oscillations (see figure 10*c*). With further increase in $\bar{u}$, we notice a transition of the system dynamics to sufficiently large-amplitude limit cycle oscillations (see figure 10*d*). It should be noted that the spikes observed in these acoustic pressure signals are the result of kicking of the acoustic modes due to vortex impingement on the bluff body (see (5.5)). Although such spikes are a feature of the model, they are not observed in the experiments. Further, in the model, the vortex impingement and the heat release rate (i.e. flame response) occur at the same time due to the assumption of a localized instantaneous heat release rate. These aspects of the model could be improved upon by incorporating equations that describe flame behaviour and its interaction with vortices and acoustics, and can be taken up in future studies of the system.

The synchronization features of the signals from the coupled oscillators, namely the acoustic pressure in the duct (p') and the circulation at the inlet step (Γ), obtained from the model are characterized by using the statistical measure of synchrony based on the RPs (Romano *et al.* 2005).

Figure 11 shows plots of the probability of recurrence ($P(\tau)$) of the phase space trajectory in the embedded phase space at different values of the time lag (τ). In the case of an aperiodic state of oscillations (figure 11*a*), the plot of $P(\tau)$ for both of the signals shows a mismatch in the locations as well as heights of the peaks, confirming their desynchronized nature. When the system enters a state of low-amplitude limit cycle oscillations, we observe the locking of positions of peaks in the plot of $P(\tau)$ of acoustic pressure and circulation. However, the heights of the peaks do not match perfectly. This shows that the system is likely to be in a state of PS. At the onset of large-amplitude limit cycle oscillations in the system, we notice almost perfect locking of both the positions and the heights of the peaks of $P(\tau)$, suggesting the presence

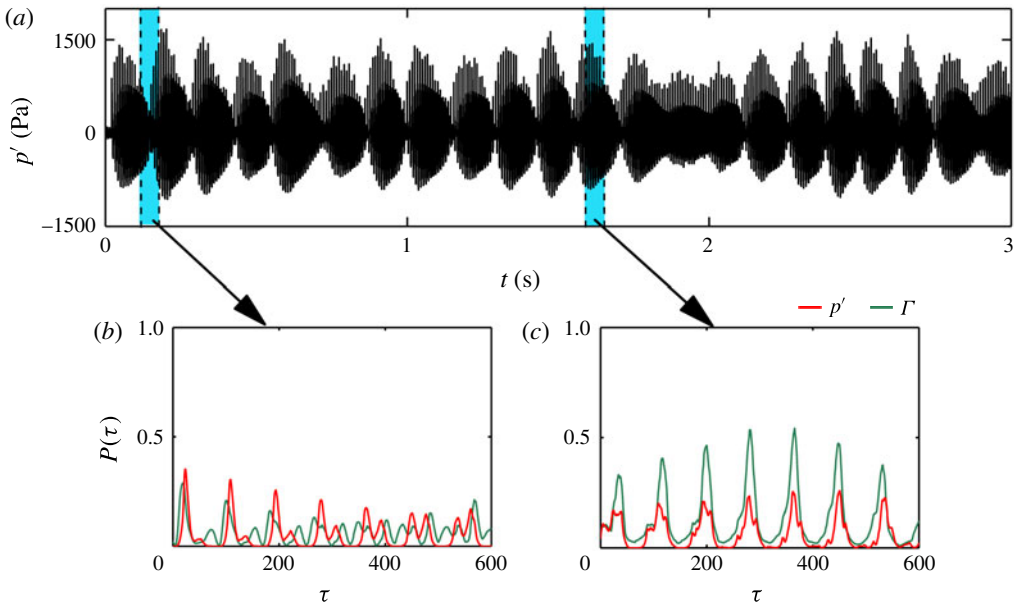

FIGURE 12. (Colour online) (*a*) The time series of the acoustic pressure (p') acquired during an intermittency state ($\bar{u} = 10.2$ m s^{-1}) from the model. (*b*,*c*) Plots of $P(\tau)$, obtained for p' (green colour) and Γ (red colour), corresponding to the regions (highlighted by blue colour) of aperiodic and periodic oscillations respectively. The parameters used in plotting (*b*,*c*) are embedding dimension = 12, time delay = 2 ms and recurrence threshold = 20 % of the maximum size of the attractor. The data window contains 4000 points (shown for 600 points).

of GS of the two oscillators in the system. These observations conform to what we observed in the experiments (refer to figure 4).

Figure 12 shows the synchronization features of the intermittency signal of p' and Γ obtained from the model. The plots of the probability of recurrence $P(\tau)$ obtained during aperiodic and periodic epochs of the intermittent oscillations are shown in figures 12(*b*) and 12(*c*) respectively. In the model, we observe smaller durations of the aperiodic oscillations compared with those of the bursts of periodic oscillations during intermittency (see figure 12*a*). During the periodic epochs of the signal (figure 12*c*), we notice locking of the positions of the peaks of $P(\tau)$ without locking of their heights, which confirms their PS nature. On the other hand, during the aperiodic epochs of the signal (figure 12*b*), locking of the positions as well as the heights of the peaks of $P(\tau)$ is absent, hinting at their desynchronized nature. This suggests that the intermittency in the model corresponds to the IPS state, which is the same as what we observed in the experiments (refer to figure 5).

As before, we study the properties of the limit cycle oscillations observed during PS and GS states in the model by examining the kicking times (see figure 13). The kicking time corresponds to the time instant at which a vortex shed from the step reaches the location of the bluff body (refer to figure 9). It should be recalled that on the impingement of a vortex, an acoustic wave travels upstream and affects the vortex shedding process, which affects the subsequent kicking times. Therefore, kicking times contain information about the dynamics of the system. Figure 13 illustrates the difference in two consecutive kicking times (normalized by the period

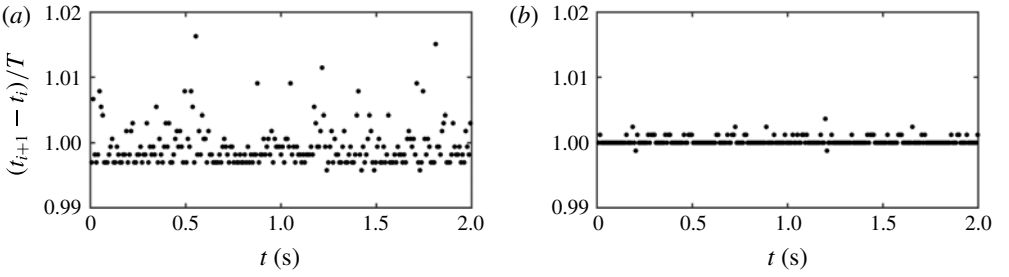

FIGURE 13. (*a*,*b*) Plots corresponding to the difference between consecutive kicking times, normalized by the respective signal period, obtained from the model. Each point in the plot corresponds to the difference in the kicking time due to two consecutively shed vortices. The time instant at which a shed vortex reaches the bluff body location is called the kicking time, as this event leads to impulsive forcing of the acoustic oscillator through the heat release rate. The plot of kicking times (*a*) corresponds to the PS state obtained at $\bar{u} = 10.41$ m s^{-1} and the plot (*b*) corresponds to the GS state obtained at $\bar{u} = 10.6$ m s^{-1}.

of the respective signal) observed during PS and GS states in the system. In the case of PS (figure 13*a*), we notice more distributed kicking times around the dominant time period as opposed to what is observed during GS (figure 13*b*). This reasserts that when the kicking times are more ordered, i.e. the time of kicking matches the dominant period of the signal, the system exhibits large-amplitude limit cycle oscillations. This, in turn, ensures that the acoustic feedback is stronger. These observations are the same as what we observed in the experiments.

6. Conclusions

In this paper, we describe the dynamical transition of a turbulent bluff-body-stabilized backward-facing step combustor using a framework of synchronization theory. We focus on the transition of this system from a state of stable operation (or combustion noise: low-amplitude aperiodic fluctuations) to a state of unstable operation (or limit cycle oscillations) in the combustor. Using a measure based on RPs, we show that the thermoacoustic instability in the system involving turbulent flow is a synchronization phenomenon of two mutually coupled non-identical oscillators, namely the acoustic field in the confinement and the turbulent reactive flow present in the system. We show that a bidirectional coupling exists between these oscillators, which is responsible for their transition from a non-synchronous state of aperiodic oscillations to a perfectly synchronous state of periodic oscillations with a variation in the mean velocity of flow. Using the theory of synchronization, we provide a new description of the intermittency route to thermoacoustic instability in a turbulent combustion system. We observe that the system dynamics culminates in a state of GS, having gone through IPS and PS. During IPS, the oscillators are periodic in the synchronized phase while harbouring aperiodicity in the desynchronized phase. In addition, our theoretical model qualitatively captures the features of synchronization observed in the experiments. Thus, we present experimental and theoretical evidence of synchronization in a practical combustion system, wherein the desynchronized coupled chaotic oscillators transition from a chaotic to a periodic state as they synchronize.

We further characterize the distinguishing features of PS and GS states. We show that these two states correspond to two different types of limit cycle oscillation: one that is weakly correlated while the other is strongly correlated. The observation of the

presence of two types of limit cycle oscillation seems to have been overlooked in the study of thermoacoustic instability in turbulent combustion systems. Using a measure of the linear correlation coefficient between the signals of the coupled subsystems, we show that the transition from the PS to the GS state results in a significant increase in the linear correlation of the signals. From the observation of kicking times, we show that, during PS, the difference between two consecutive kicking times is widely distributed, compared with what is seen during GS. In addition, we observe a wide variation in the cycle-to-cycle amplitude of the acoustic pressure signals during PS, whereas the amplitude is nearly constant during GS. Thus, during GS, a stronger form of lock-in mechanism is observed in the system.

Thus, our approach to viewing thermoacoustic instability in combustors with the turbulent flow as a synchronization phenomenon is a step towards an understanding of the complex nonlinear interactions occurring between the coupled subsystems of such combustors. As a prerequisite for examining the synchronization phenomenon in a system of coupled oscillators is that the oscillators should be distinct and self-sustained, it is not clear at the outset whether such an approach of mutual synchronization could be further extended to thermoacoustic systems involving laminar flows. In the class of systems with turbulent flow, due to the intrinsic hydrodynamic fluctuations, there will always be an oscillatory behaviour in the flow. Hence, the framework of synchronization is valid for such systems, as we show in the present study. On the other hand, in the case of laminar systems, such as Rijke tube and ducted laminar premixed flames, we do see synchronous behaviour between the acoustic field and the heat release rate oscillations at the onset of thermoacoustic instability. However, in the absence of noise or inherent fluctuations in the flow during a steady state, the acoustic field is silent (hardly any perceptible pressure or velocity fluctuations) and the heat release rate field is not oscillatory (no perceptible oscillations in the flame or the heat release rate). As a consequence, the use of synchronization theory to describe the route to thermoacoustic instability in laminar combustors may not be fruitful.

Furthermore, this approach of synchronization theory can probably be used in other real fluid mechanical systems involving turbulent flow, in which the coupled response of two or more interacting subsystems leads to an unstable phenomenon of flow-induced vibrations. In such systems, the quantitative analysis of synchronization phenomena is still an open topic of research.

Acknowledgements

We acknowledge ONRG for the financial support (Contract Monitor: Dr R. Kolar; grant no. N62909-14-1-N299). We would like to thank Dr D. V. Senthilkumar, Dr S. S. Gunthe and Dr K. Balasubramanian for the discussion on the manuscript. We are also grateful to Mr N. B. George for the help provided in conducting experiments and Mr Thilagraj for providing the schematic of the experimental set-up. We finally thank Dr S. Mondal for the fruitful discussion that happened during the course of the manuscript preparation. S.A.P. is grateful to IIT Madras and MHRD, India for providing the scholarship for the doctoral degree.

REFERENCES

ABARBANEL, H. 1996 *Analysis of Observed Chaotic Data*. Springer.

ANANTHKRISHNAN, N., DEO, S. & CULICK, F. E. 2005 Reduced-order modeling and dynamics of nonlinear acoustic waves in a combustion chamber. *Combust. Sci. Technol.* **177** (2), 221–248.

BALUSAMY, S., LI, L. K., HAN, Z., JUNIPER, M. P. & HOCHGREB, S. 2015 Nonlinear dynamics of a self-excited thermoacoustic system subjected to acoustic forcing. *Proc. Combust. Inst.* **35** (3), 3229–3236.

BELLOWS, B., HREIZ, A. & LIEUWEN, T. 2008 Nonlinear interactions between forced and self-excited acoustic oscillations in premixed combustor. *J. Propul. Power* **24** (3), 628–631.

BLASIUS, B., AMIT, H. & LEWI, S. 1999 Complex dynamics and phase synchronization in spatially extended ecological systems. *Nature* **399**, 354–359.

BLEKHMAN, I. I., LANDA, P. S. & ROSENBLUM, M. G. 1995 Synchronization and chaotization in interacting dynamical systems. *Appl. Mech. Rev.* **48**, 733–752.

BLEVINS, R. D. 1985 The effect of sound on vortex shedding from cylinders. *J. Fluid Mech.* **161**, 217–237.

BOCCALETTI, S., KURTHS, J., OSIPOV, G., VALLADARES, D. L. & ZHOU, C. S. 2002 The synchronization of chaotic systems. *Phys. Rep.* **366** (1), 1–101.

BOVE, I., BOCCALETTI, S., BRAGARD, J., KURTHS, J. & MANCINI, H. 2004 Frequency entrainment of nonautonomous chaotic oscillators. *Phys. Rev.* E **69** (1), 016208.

BRODA, J. C., SEO, S., SANTORO, R. J., SHIRHATTIKAR, G. & YANG, V. 1998 An experimental study of combustion dynamics of a premixed swirl injector. *Proc. Combust. Inst.* **27** (2), 1849–1856.

CAO, L. 1997 Practical method for determining the minimum embedding dimension of a scalar time series. *Physica* D **110** (1), 43–50.

CHAKRAVARTHY, S. R., SIVAKUMAR, R. & SHREENIVASAN, O. J. 2007 Vortex-acoustic lock-on in bluff-body and backward-facing step combustors. *Sadhana* **32** (1–2), 145–154.

CRUMP, J. E., SCHADOW, K. C., YANQ, V. & CULICK, F. E. C. 1986 Longitudinal combustion instabilities in ramjet engines: identification of acoustic modes. *J. Propul. Power* **2**, 105–109.

CULICK, F. E. C. 1976 Nonlinear behavior of acoustic waves in combustion chambers – I. *Acta Astron.* **3** (9), 715–734.

CULICK, F. E. C. 1994 Some recent results for nonlinear acoustics in combustion chambers. *AIAA J.* **32** (1), 146–169.

DATTA, S., MONDAL, S., MUKHOPADHYAY, A., SANYAL, D. & SEN, S. 2009 An investigation of nonlinear dynamics of a thermal pulse combustor. *Combust. Theor. Model.* **13** (1), 17–38.

DOWLING, A. P. 1997 Nonlinear self-excited oscillations of a ducted flame. *J. Fluid Mech.* **346**, 271–290.

ECKMANN, J. P., KAMPHORST, S. O. & RUELLE, D. 1987 Recurrence plots of dynamical systems. *Europhys. Lett.* **4** (9), 973–977.

FRASER, A. M. & SWINNEY, H. L. 1986 Independent coordinates for strange attractors from mutual information. *Phys. Rev.* A **33** (2), 1134.

FUJISAKA, H. & YAMADA, T. 1983 Stability theory of synchronized motion in coupled-oscillator systems. *Prog. Theor. Phys.* **69** (1), 32–47.

GABOR, D. 1946 Theory of communication. *J. Inst. Electr. Engng* **93** (26), 429–441.

GONZALEZ-MIRANDA, J. M. 2002 Amplitude envelope synchronization in coupled chaotic oscillators. *Phys. Rev.* E **65** (3), 036232.

GOTODA, H., NIKIMOTO, H., MIYANO, T. & TACHIBANA, S. 2011 Dynamic properties of combustion instability in a lean premixed gas-turbine combustor. *Chaos* **21**, 013124.

GOTODA, H., SHINODA, Y., KOBAYASHI, M. & OKUNO, Y. 2014 Detection and control of combustion instability based on the concept of dynamical system theory. *Phys. Rev.* E **89**, 022910.

GREEN, S. I. 1995 Vortex–structure interaction. In *Fluid Vortices*, chap. XII, pp. 533–574. Kluwer Academic.

GRIFFIN, O. M. & HALL, M. S. 1991 Review – vortex shedding lock-on and flow control in bluff body wakes. *Trans. ASME J. Fluids Engng* **113** (4), 526–537.

GRIFFIN, O. M. & RAMBERG, S. E. 1974 The vortex street wakes of vibrating cylinders. *J. Fluid Mech.* **66**, 553–576.

GUETHE, F., GUYOT, D., SINGLA, G., NOIRAY, N. & SCHUERMANS, B. 2012 Chemiluminescence as diagnostic tool in the development of gas turbines. *Appl. Phys.* B **107** (3), 619–636.

GUETHE, F. & SCHUERMANS, B. 2007 Phase-locking in post-processing for pulsating flames. *Meas. Sci. Technol.* **18** (9), 3036.

GUNNOO, H., ABCHA, N. & EZERSKY, A. 2016 Frequency lock-in and phase synchronization of vortex shedding behind circular cylinder due to surface waves. *Phys. Lett.* A **380** (7), 863–868.

HEAGY, J. F., CARROLL, T. L. & PECORA, L. M. 1994 Synchronous chaos in coupled oscillator systems. *Phys. Rev.* E **50** (3), 1874.

IKEDA, Y., KOJIMA, J. & HASHIMOTO, H. 2002 Local chemiluminescence spectra measurements in a high-pressure laminar methane/air premixed flame. *Proc. Combust. Inst.* **29**, 1495–1501.

JAHNKE, C. C. & CULICK, F. E. 1994 Application of dynamical systems theory to nonlinear combustion instabilities. *J. Propul. Power* **10** (4), 508–517.

KABIRAJ, L., SAURABH, A., WAHI, P. & SUJITH, R. I. 2012*a* Route to chaos for combustion instability in ducted laminar premixed flames. *Chaos* **22**, 023129.

KABIRAJ, L. & SUJITH, R. I. 2012 Nonlinear self-excited thermoacoustic oscillations: intermittency and flame blowout. *J. Fluid Mech.* **713**, 376–397.

KABIRAJ, L., SUJITH, R. I. & WAHI, P. 2012*b* Investigating the dynamics of combustion-driven oscillations leading to lean blowout. *Fluid Dyn. Res.* **44**, 031408.

KASHINATH, K., WAUGH, I. C. & JUNIPER, M. P. 2014 Nonlinear self-excited thermoacoustic oscillations of a ducted premixed flame: bifurcations and routes to chaos. *J. Fluid Mech.* **761**, 399–430.

KELLER, J. O., VANEVELD, L., KORSCHELT, D., HUBBARD, G. L., GHONIEM, A. F., DAILY, J. W. & OPPENHEIM, A. K. 1982 Mechanism of instabilities in turbulent combustion leading to flashback. *AIAA J.* **20** (2), 254–262.

KOCAREV, L. & PARLITZ, U. 1995 General approach for chaotic synchronization with application to communication. *Phys. Rev. Lett.* **74**, 5028–5031.

LAKSHMANAN, M. & SENTHILKUMAR, D. V. 2011 *Dynamics of Nonlinear Time-delay Systems*. Springer.

LEI, S. & TURAN, A. 2009 Nonlinear/chaotic behaviour in thermo-acoustic instability. *Combust. Theor. Model.* **13** (3), 541–557.

LEON, G. 2001 Synchronization and rhythmic processes in physiology. *Nature* **410**, 277–284.

LIEUWEN, T. & YANG, V. 2005 *Combustion Instabilities in Gas Turbine Engines: Operational Experience, Fundamental Mechanisms, and Modeling*. American Institute of Aeronautics and Astronautics.

LIEUWEN, T. C. 2002 Experimental investigation of limit cycle oscillations in an unstable gas turbine combustor. *J. Propul. Power* **18**, 61–67.

LIEUWEN, T. C. 2003*a* Modeling premixed combustion–acoustic wave interactions: a review. *J. Propul. Power* **19** (5), 765–781.

LIEUWEN, T. C. 2003*b* Statistical characteristics of pressure oscillations in a premixed combustor. *J. Sound Vib.* **260** (1), 3–17.

LIEUWEN, T. C. 2005 Online combustor stability margin assessment using dynamic pressure data. *Trans. ASME: J. Engng Gas Turbines Power* **127** (3), 478–482.

MACQUISTEN, M. A. & DOWLING, A. P. 1993 Low-frequency combustion oscillations in a model afterburner. *Combust. Flame* **94** (3), 253–264.

MARWAN, N. 2011 How to avoid potential pitfalls in recurrence plot based data analysis. *Intl J. Bifurcation Chaos* **21** (04), 1003–1017.

MARWAN, N., ROMANO, M. C., THIEL, M. & KURTHS, J. 2007 Recurrence plots for the analysis of complex systems. *Phys. Rep.* **438** (5), 237–329.

MATVEEV, K. I. & CULICK, F. E. C. 2003 A model for combustion instability involving vortex shedding. *Combust. Sci. Technol.* **175**, 1059–1083.

MCMANUS, K. R., POINSOT, T. & CANDEL, S. M. 1993 A review of active control of combustion instabilities. *Prog. Energy Combust. Sci.* **16**, 1–29.

MONDAL, S., UNNI, V. R. & SUJITH, R. I. 2017 Onset of thermoacoustic instability in turbulent combustors: an emergence of synchronized periodicity through formation of chimera-like states. *J. Fluid Mech.* **811**, 659–681.

MURUGESAN, M. & SUJITH, R. I. 2015*a* Combustion noise is scale-free: transition from scale-free to order at the onset of thermoacoustic instability. *J. Fluid Mech.* **772**, 225–245.

MURUGESAN, M. & SUJITH, R. I. 2015*b* Intermittency in combustion dynamics. In *51st AIAA/SAE/ASEE Joint Propulsion Conference*. *AIAA Paper* 2015-3967.

NAIR, V. & SUJITH, R. I. 2013 Identifying homoclinic orbits in the dynamics of intermittent signals through recurrence quantification. *Chaos* **23**, 033136.

NAIR, V. & SUJITH, R. I. 2014 Multifractality in combustion noise: predicting an impending instability. *J. Fluid Mech.* **747**, 635–655.

NAIR, V. & SUJITH, R. I. 2015 A reduced-order model for the onset of combustion instability: physical mechanisms for intermittency and precursors. *Proc. Combust. Inst.* **35** (3), 3193–3200.

NAIR, V., THAMPI, G., KARUPPASAMY, S., GOPALAN, S. & SUJITH, R. I. 2013 Loss of chaos in combustion noise as a precursor for impending instability. *Intl J. Spray Combust. Diag.* **5**, 273–290.

NAIR, V., THAMPI, G. & SUJITH, R. I. 2014 Intermittency route to thermoacoustic instability in turbulent combustors. *J. Fluid Mech.* **756**, 470–487.

NOIRAY, N. & SCHUERMANS, B. 2012 Theoretical and experimental investigations on damper performance for suppression of thermoacoustic oscillations. *J. Sound Vib.* **331** (12), 2753–2763.

OSIPOV, G. V., HU, B., ZHOU, C., IVANCHENKO, M. V. & KURTHS, J. 2003 Three types of transitions to phase synchronization in coupled chaotic oscillators. *Phys. Rev. Lett.* **91** (2), 024101.

PAWAR, S. A., VISHNU, R., VADIVUKKARASAN, M., PANCHAGNULA, M. V. & SUJITH, R. I. 2016 Intermittency route to combustion instability in a laboratory spray combustor. *Trans. ASME: J. Engng Gas Turbines Power* **138** (4), 041505.

PIKOVSKY, A., ROSENBLUM, M. & KURTHS, J. 2003 *Synchronization: A Universal Concept in Nonlinear Science*. Cambridge University Press.

POINSOT, T. J., TROUVE, A. C., VEYNANTE, D. P., CANDEL, S. M. & ESPOSITO, E. J. 1987 Vortex-driven acoustically coupled combustion instabilities. *J. Fluid Mech.* **177**, 265–292.

PUTNAM, A. A. 1971 *Combustion-Driven Oscillations in Industry*. Elsevier.

PYRAGAS, K. 1998 Properties of generalized synchronization of chaos. *Nonlinear Anal. Model.* **3**, 1–29.

RAYLEIGH, J. S. W. 1878 The explanation of certain acoustic phenomena. *Nature* **18** (455), 319–321.

ROGERS, D. E. 1956 A mechanism for high-frequency oscillation in ramjet combustors and afterburners. *Jet Propul.* **26** (6), 456–462.

ROMANO, M. C., THIEL, M., KURTHS, J., KISS, I. Z. & HUDSON, J. L. 2005 Detection of synchronization for non-phase-coherent and non-stationary data. *Europhys. Lett.* **71** (3), 466.

ROSENBLUM, M. G., PIKOVSKY, A. S. & KURTHS, J. 1996 Phase synchronization of chaotic oscillators. *Phys. Rev. Lett.* **76** (11), 1804.

ROSENBLUM, M. G., PIKOVSKY, A. S. & KURTHS, J. 1997 From phase to lag synchronization in coupled chaotic oscillators. *Phys. Rev. Lett.* **78** (22), 4193.

ROY, R. & THORNBURG, K. S. JR. 1994 Experimental synchronization of chaotic lasers. *Phys. Rev. Lett.* **72** (13), 2009–2012.

RULKOV, N. F., SUSHCHIK, M. M., TSINGRING, L. S. & ABARBANEL, H. D. I. 1995 Generalized synchronition of chaos in directionally coupled chaotic systems. *Phys. Rev.* E **51** (2), 980.

SCHADOW, K. C. & GUTMARK, E. 1992 Combustion instability related to vortex shedding in dump combustors and their passive control. *Prog. Energy Combust. Sci.* **18** (2), 117–132.

SCHINKEL, S., DIMIGEN, O. & MARWAN, N. 2008 Selection of recurrence threshold for signal detection. *Eur. Phys. J. Spec. Top.* **164** (1), 45–53.

SCHREIBER, I. & MAREK, M. 1982 Strange attractor in coupled reaction diffusion cells. *Physica* D **5** (2), 258–272.

SESHADRI, A., NAIR, V. & SUJITH, R. I. 2016 A reduced-order deterministic model describing intermittency route to combustion instability. *Combust. Theor. Model.* **20** (3), 441–456.

SHANBHOGUE, S. J., HUSAIN, S. & LIEUWEN, T. 2009 Lean blowoff of bluff body stabilized flames: scaling and dynamics. *Prog. Energy Combust. Sci.* **35** (1), 98–120.

SIVAKUMAR, R. & CHAKRAVARTHY, S. R. 2008 Experimental investigation of the acoustic field in a bluff-body combustor. *Intl J. Aeroacoust.* **7** (3–4), 267–299.

SMITH, D. A. & ZUKOSKI, E. E. 1985 Combustion instability sustained by unsteady vortex combustion. In *AIAA/SAE/ASME/ASEE 21st Joint Propulsion Conference. AIAA Paper* 85-1248.

STERLING, J. D. 1993 Nonlinear analysis and modelling of combustion instabilities in a laboratory combustor. *Combust. Sci. Technol.* **89** (1–4), 167–179.

STERLING, J. D. & ZUKOSKI, E. E. 1987 Longitudinal mode combustion instabilities in a dump combustor. In *25th Aerospace Sciences Meeting, Reno, NV. AIAA Paper* 87-0220.

STRAHLE, W. C. 1978 Combustion noise. *Prog. Energy Combust. Sci.* **4** (3), 157–176.

SUBRAMANIAN, P. 2011 Dynamical systems approach to the investigation of thermoacoustic instabilities. PhD thesis, Indian Institute of Technology Madras.

SUBRAMANIAN, P., MARIAPPAN, S., SUJITH, R. I. & WAHI, P. 2010 Bifurcation analysis of thermoacoustic instability in a horizontal Rijke tube. *Intl J. Spray Combust. Diag.* **2** (4), 325–355.

SUJITH, R. I., JUNIPER, M. P. & SCHMID, P. J. 2016 Non-normality and nonlinearity in thermoacoustic instabilities. *Intl J. Spray Combust. Diag.* **8** (2), 119–146.

SUNGWOO, A., PARK, C. & RUBCHINSKY, L. L. 2011 Detecting the temporal structure of intermittent phase locking. *Phys. Rev.* E **84**, 016201.

TAKENS, F. 1980 Detecting strange attractors in turbulence. In *Dynamical Systems and Turbulence, Warwick* (ed. R. David & L.-S. Young), Lecture Notes in Mathematics, vol. 898, pp. 366–381. Springer.

THUMULURU, S. K. & LIEUWEN, T. 2009 Characterization of acoustically forced swirl flame dynamics. *Proc. Combust. Inst.* **32** (2), 2893–2900.

TONY, J., GOPALAKRISHNAN, E. A., SREELEKHA, E. & SUJITH, R. I. 2015 Detecting deterministic nature of pressure measurements from a turbulent combustor. *Phys. Rev.* E **92** (6), 062902.

UNNI, V. R. & SUJITH, R. I. 2015 Multifractal characteristics of combustor dynamics close to lean blowout. *J. Fluid Mech.* **784**, 30–50.

UNNI, V. R. & SUJITH, R. I. 2015 Flame dynamics during intermittency in a turbulent combustor. *Proc. Combust. Inst.* **36** (3), 3791–3798.

VENKATARAMAN, K. K., PRESTON, L. H., SIMONS, D. W., LEE, B. J., LEE, J. G. & SANTAVICCA, D. A. 1999 Mechanism of combustion instability in a lean premixed dump combustor. *J. Propul. Power* **15** (6), 909–918.

WELCH, P. 1967 The use of fast Fourier transform for the estimation of power spectra: a method based on time averaging over short, modified periodograms. *IEEE Trans. Acoust. Speech* **15** (2), 70–73.

WEN, W., KISS, I. Z. & HUDSON, J. L. 2001 Clustering of arrays of chaotic chemical oscillators by feedback and forcing. *Phys. Rev. Lett.* **86**, 4954.

WILHITE, J. M., DOLAN, B. J., KABIRAJ, L., GOMEZ, R. V. & GUTMARK, E. J. 2016 Analysis of combustion oscillations in a staged MLDI burner using decomposition methods and recurrence analysis. In *54th AIAA Aerospace Sciences Meeting. AIAA SciTech AIAA* 2016-1156.

WILLIAMSON, C. H. K. & ROSHKO, A. 1988 Vortex formation in the wake of an oscillating cylinder. *J. Fluids Struct.* **2**, 355–381.

YALÇINKAYA, T. & LAI, Y. C. 1997 Phase characterization of chaos. *Phys. Rev. Lett.* **79** (20), 3885.

YU, H. K., TROUVE, A. & DAILY, J. W. 1991 Low-frequency pressure oscillations in a model ramjet combustor. *J. Fluid Mech.* **232**, 47–72.

ZDRAVKOVICH, M. M. 1982 Modification of vortex shedding in the synchronization range. *Trans. ASME J. Fluids Engng* **104** (4), 513–517.

ZINN, B. T. & LORES, M. E. 1971 Application of the Galerkin method in the solution of non-linear axial combustion instability problems in liquid rockets. *Combust. Sci. Technol.* **4**, 269–278.